

RoLEX: A LoRa-based Rotation Speed Measurement System for Ubiquitous Long-distance Monitoring Applications

Keran Li^{ID}, Student Member, IEEE, Haipeng Dai^{ID}, Senior Member, IEEE, Wei Wang^{ID}, Member, IEEE,
 Junlong Chen^{ID}, Jiliang Wang^{ID}, Senior Member, IEEE, Shuai Tong^{ID}, Meng Li^{ID}, Member, IEEE,
 Lei Wang^{ID}, Member, IEEE, Haoran Wang^{ID}, Guihai Chen^{ID}, Fellow, IEEE

Abstract—Rotation is a fundamental form of motion and rotation speed measurement holds paramount importance for assessing the health and performance of machinery with rotating components. However, existing measurement systems often face challenges such as limited measurement distance, low accuracy, and complex installation or maintenance processes. In this paper, we propose RoLEX, a LoRa-based rotation speed measurement system for long-distance and contactless monitoring of rotating machinery in ubiquitous scenarios. RoLEX employs a novel Signal Selection method to eliminate chirp interference and adapt to varying rotation speeds, along with a Boost Sensing method to enhance sampling rates and an advanced feature processing algorithm for precise rotation speed estimation and tracking. Comprehensive experiments validate that RoLEX achieves a measurement distance of 50 m, approximately 17 times farther than the latest wireless rotation speed measurement systems. Moreover, RoLEX is robust to interference and obstructions (including through-wall scenarios) and achieves an average measurement error less than 0.69% across different rotation speeds (100 - 5100 Revolutions Per Minute). For tracking performance, RoLEX achieves a relative error less than 2.8% in 90% of cases. We also present a case study to highlight RoLEX’s practical applicability in real-world scenarios.

Index Terms—LoRa Sensing, Mobile Computing, Rotation Speed Measurement, Signal Processing.

Received 5 April 2025; revised 12 September 2025; accepted 14 October 2025. This work was supported in part by the National Key R&D Program of China under Grant No. 2023YFB4502400, in part by the National Natural Science Foundation of China under Grant U22A2031, U24B20153, 62272223, 61872178, 62272213, in part by the New Generation Information Technology Innovation Project 2023 (2023IT196), in part by the Fundamental Research Funds for the Central Universities under Grant No. 2024300349, in part by the Collaborative Innovation Center of Novel Software Technology and Industrialization, Nanjing University, in part by the Jiangsu High-level Innovation and Entrepreneurship (Shuangchuang) Program, and in part by the Postgraduate Research & Practice Innovation Program of Jiangsu Province under Grant KYCX24_0243. (Corresponding authors: Haipeng Dai and Wei Wang.)

Keran Li, Haipeng Dai, Wei Wang, Junlong Chen, Meng Li, Haoran Wang and Guihai Chen are with the School of Computer Science, Nanjing University, Nanjing, Jiangsu 210023, China and also with the State Key Laboratory for Novel Software Technology, Nanjing University, Nanjing, Jiangsu 210023, China. (e-mail: keranli@mail.nju.edu.cn; haipengdai@nju.edu.cn; ww@nju.edu.cn; 522023330012@mail.nju.edu.cn; meng@nju.edu.cn; 221220146@mail.nju.edu.cn; gchen@nju.edu.cn.)

Jiliang Wang and Shuai Tong are with the School of Software and BNRIst, Tsinghua University, Beijing 100084, China. (e-mail: jiliangwang@tsinghua.edu.cn; tongshuai.ts@gmail.com.)

Lei Wang is with the School of Future Science and Engineering, Soochow University, Suzhou, Jiangsu 215222, China. (e-mail: wanglei@suda.edu.cn.)

I. INTRODUCTION

ROTATION is a fundamental form of motion prevalent in both daily lives [1], [2] and industrial scenarios [3]–[5]. Measuring rotation speed (RS) is vital to monitoring the health of rotating machinery, enabling the assessment of performance and the early detection of anomalies or potential failures. For instance, in a machine shop, operators routinely monitor the rotation speed of spindles to gauge operational status for failure detection [6]. Similarly, precise assessment of wheel rotation speed has become a standard procedure in automobile inspections [7]. As rotating machinery is central to many sectors, including manufacturing and transportation, ensuring its reliable operation through precise rotation speed measurement is key to optimizing overall system performance.

To address the diverse requirements of RS measurement, various systems have been developed, which can be broadly categorized into contact-based and contactless-based systems. Contact-based systems [8] require physical contact with the rotating target, posing significant safety risks, especially for high-speed machinery. As a result, they are typically limited to small, low-speed objects. Contactless-based systems, on the other hand, rely on electromagnetic, optical, or wireless signals. Electromagnetic systems [5], [9] have a short sensing range (typically less than 10 cm), making them unsuitable for large-scale or hazardous scenarios. Optical systems [10], [11] require strict lighting conditions and are prone to failures in low-light or obstructed environments. Wireless systems, such as acoustic-based systems [1] and RF-based systems [4], [12], overcome some of these limitations but also face notable challenges. Acoustic-based systems are highly susceptible to environmental noise, while RF-based systems still struggle with limited sensing distances (0.8 m in [1] and 3 m in [12]). Therefore, to bridge the gap, we need to develop an accurate and long-distance rotation speed measurement system.

In this paper, we propose RoLEX, a LoRa-based rotation speed measurement system for long-distance monitoring of rotating machinery in ubiquitous scenarios. To the best of our knowledge, RoLEX is the first system to leverage LoRa signal for long-distance, contactless and accurate rotation speed measurement, and achieves outstanding performance

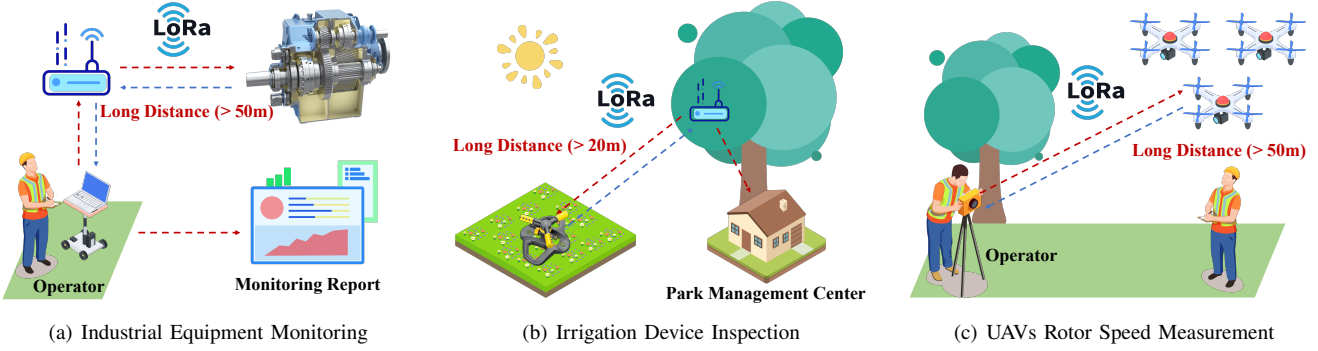


Fig. 1. Typical Applications of RoLEX

even in the presence of environmental interference and obstructions. LoRa's inherent properties make it well suited for long-distance and high-precision rotation speed measurement. Unlike traditional RF or acoustic sensing technologies, LoRa employs chirp spread spectrum (CSS) modulation [13], [14], which not only offers strong resistance to multipath fading and environmental noise, but also produces highly stable linear frequency sweeps. Moreover, such chirp structures are sensitive to phase shifts induced by rotating targets, enabling RoLEX to accurately extract rotational features even under low-SNR conditions. These advantages allow RoLEX to achieve long-distance, contactless, and accurate rotation speed measurement in environments where other wireless methods struggle.

As shown in the Fig. 1, RoLEX has many typical applications. RoLEX can be utilized in industrial settings to remotely monitor the rotation speed of heavy machinery [4] (Fig.1(a)). Beyond industrial applications, Fig.1(b) showcases how RoLEX can be deployed in parks to remotely track the operational status of rotary irrigation systems on lawns [14]. Furthermore, in UAV operations (Fig.1(c)), RoLEX reliably monitors rotor speeds in real-time, enabling precise diagnostics of flight performance and early anomaly detection [15].

Existing LoRa-based sensing systems typically target low-frequency, slowly varying motions (*e.g.*, human activity or vital signs) [16]–[18] and are not designed to handle the high-frequency, fast-changing dynamics in rotation speed measurement. **Therefore, implementing RoLEX introduces three unique challenges.** Firstly, the potential interference between the chirp frequency (we call it “Boundary Frequency”) and the target’s rotation speed must be addressed, as they may both reside within similar frequency ranges, complicating signal separation. Secondly, LoRa signals have inherently low chirp rates, limited by a maximum chirp length of 32.8 ms (about 30 Hz). This restricts measurements to around 900 RPM (15 Hz), while target rotation speeds can be much higher (1000 RPM–5000 RPM). Overcoming this limitation to sense high-frequency rotation motion is a key challenge. Thirdly, existing LoRa-based systems lack the capability to capture high-frequency motion features such as rapid phase shifts. This poses a significant challenge in accurately extracting and tracking rotation speed, requiring novel signal processing techniques tailored to LoRa’s modulation characteristics.

To address these challenges, we develop a theoretical model and a series of novel methods for RoLEX, which enable RoLEX to accurately measure a wide range of rotation speeds

over long distances. For the first challenge, we propose a new Signal Selection method to reduce the interference. Specifically, by performing an initial classification of the rotation speed, RoLEX can select the most appropriate signal which avoids interference from the Boundary Frequency. For the second challenge, we propose a Boost Sensing method to increase sensing sampling rate, enabling the sensing of high-frequency rotational motion. Specifically, RoLEX first segments the signal, and then uses the Fast Fourier Transform (FFT) operation to further concentrate the frequency energy of each signal segment, which can improve the sensing sampling rate of RoLEX. For the third challenge, we use the phase changes as the signal features for rotation sensing, as the rotation of the target induces these changes. Specifically, RoLEX extracts and accumulates the phase information of each signal segment, which is highly correlated with the rotation. Further, we propose a novel Feature Processing method to calculate and track the rotation speed accurately.

Our main contributions are as follows:

- We propose and implement a novel LoRa-based rotation speed sensing system named RoLEX. To the best of our knowledge, RoLEX is the first system to leverage LoRa signal for long-distance, contactless and accurate rotation speed measurement, and exhibits robust performance even in the presence of interference and obstructions.
- We establish the theoretical model and propose three novel methods for RoLEX: (i) a Signal Selection method to reduce the interference caused by Boundary Frequency; (ii) a Boost Sensing method to cover a wide rotation speed range; (iii) a Feature Processing method to calculate and track the rotation speed accurately.
- Experimental results show that RoLEX can achieve rotation sensing with a distance of up to 50 m, which is nearly 17 times that of the latest sensing technology [12]. Meanwhile, RoLEX can cover a wide rotation speed range from 100 Revolutions Per Minute (RPM) to 5100 Revolutions Per Minute with an average measurement error less than 0.69% on a variety of rotating objects. As for tracking performance, when using different rotors, RoLEX can achieve across-range tracking with relative error less than 2.8% in 90% of cases.
- We deploy RoLEX in a practical scenario to monitor the rotation speed of a rotary irrigation device and correlate it with the corresponding water flow rate. Experimental

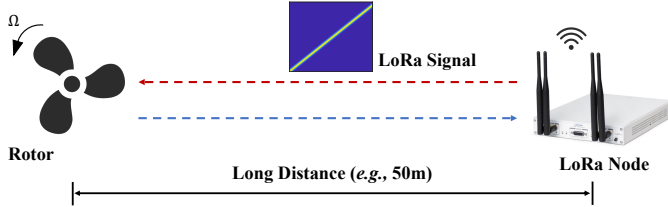


Fig. 2. System Overview of RoLEX

results demonstrate that RoLEX can achieve near real-time monitoring of the irrigation device's operational status, with a rotation speed measurement error of less than 1.67% and a latency of under 0.6 s.

The rest of the paper is organized as follows. In Sec. II, we introduce the preliminaries of LoRa sensing. Then, we introduce the theoretical model of RoLEX and how we design RoLEX in detail in Sec. III and Sec. IV, respectively. Next, we conduct extensive experiments to evaluate the performance of RoLEX in Sec. V and present a case study in Sec. VI. We discuss the limitations and potential future work in Sec. VII. Finally, we review the related work and conclude this paper in Sec. VIII and Sec. IX.

II. PRELIMINARIES

In this section, we first introduce the chirp-based modulation and demodulation technology of LoRa, and then introduce the LoRa sensing model.

A. LoRa Technology

Modulation. The upchirp sweeps linearly from frequency $f_0 = -\frac{BW}{2}$ to $\frac{BW}{2}$ over a time duration of T_{chirp} where BW is the chirp bandwidth and T_{chirp} is the chirp duration. Downchirp is exactly the opposite. The complex form [18] of LoRa symbols can be expressed as

$$\begin{aligned} S_{up}(t) &= e^{j2\pi f_0 t + j\pi k t^2}, \\ S_{down}(t) &= e^{j2\pi f_1 t - j\pi k t^2}, \end{aligned} \quad (1)$$

where $f_1 = \frac{BW}{2}$ is the initial frequency of a LoRa downchirp and $k = \frac{BW}{T_{chirp}}$ is the chirp slope [19].

Demodulation. The essence of the LoRa demodulation process is to find the decoding frequency of the chirp symbol. When performing LoRa demodulation, the received baseband upchirp signal with a fixed frequency offset component (*i.e.*, data) is multiplied by the predefined downchirp to convert it into a single-frequency signal. This operation is called dechirp. Dechirp can concentrate the energy of the chirp signal into a single frequency [19], [20], which is one of the reasons why LoRa is anti-noise and can achieve long-distance transmission. Mathematically, this process can be expressed as

$$S_{dechirp}(t) = (S_{up}(t) \cdot e^{j2\pi \Delta f t}) \cdot S_{down}(t) = e^{j2\pi \Delta f t}, \quad (2)$$

where the fixed frequency offset Δf is the decoding frequency.

B. LoRa Sensing Model

The key to using LoRa signals for environmental sensing is to obtain the signal changes caused by the propagation path. As analyzed in [18], [21], the signal will pass through multiple reflection paths during propagation and finally reach the LoRa gateway. Each path corresponds to a signal attenuation coefficient and a time delay (for the i^{th} path, the attenuation coefficient is $a_i(t)$ and the time delay is $\tau_i(t)$). To simplify the analysis, we assume the transmitted signal is upchirp and $f_0 = 0$. The signal received by the LoRa gateway can be expressed as

$$\begin{aligned} S_R(t) &= \sum_{i=1}^I a_i(t) S_T(t - \tau_i(t)) \\ &= e^{j2\pi f_c t + j\pi k t^2} \sum_{i=1}^I H_i(t), \end{aligned} \quad (3)$$

where $H_i(t) = a_i(t) e^{-j2\pi(k\tau_i(t)+f_c\tau_i(t)-k\frac{\tau_i(t)^2}{2})}$ characterizes the impact of the i^{th} path on signals and f_c is the carrier frequency of the signal.

We denote the signal changes produced by the target reflection path as $H_d(t)$ and the signal changes produced by other static object reflection paths as $H_s(t)$. After receiving the signal, the mixer in the receiver will eliminate the carrier component in the received signal. We define the raw signal used for sensing as

$$S_R'(t) = e^{j\pi k t^2} (H_s(t) + H_d(t)). \quad (4)$$

Note that the dynamic component $H_d(t)$ in Eq. (4) contains the target's motion information. Consequently, our goal is to accurately obtain $H_d(t)$ and convert it into features corresponding to the target motion for sensing.

III. RoLEX MODEL

In this section, we first give an overview of our system. Then, we establish a theoretical model and analyze the relationship between rotation and the signal features.

A. System Preview

RoLEX is a system that can accurately measure the rotation speed of the targets in a contactless manner with LoRa signals. As shown in Fig. 2, the LoRa node is placed facing the rotor. When the rotor rotates, the spatial characteristics (*e.g.*, relative distance) between the node and the rotor will change accordingly. RoLEX first transmits the LoRa signal to obtain these changes and then extracts the signal features. After that, RoLEX processes these features to calculate the corresponding rotation speed. Besides, due to the long-distance transmission capability of LoRa signals, RoLEX can measure the rotation speed over long distances.

B. Theoretical Model and Analysis

To further explain the relationship between rotation and signal features, we develop a theoretical model for RoLEX and provide a detailed analysis. For any given rotor, the primary

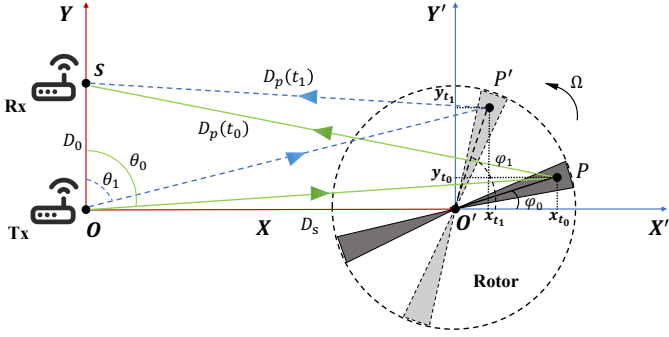


Fig. 3. Theoretical Model of RoLEX

influencing factor in the spatial domain is the relative distance between the LoRa node and the rotor. Our analysis focuses on associating the extracted signal features with the relative distance variations and the rotor's rotation speed. Since the LoRa node is omnidirectional, the placement of the node and rotor is unrestricted, allowing for maximum deployment flexibility. To simplify the analysis without loss of generality, we construct a 2-dimensional theoretical model, as shown in Fig. 3, to capture the relationship between the rotor's motion and signal features.

In Fig. 3, the coordinate system OXY is fixed relative to the Transmitter (Tx) which is located at $(0, 0)$, and Receiver (Rx) is located at $(0, S)$. The distance between them is D_0 . Another coordinate system $O'X'Y'$ is fixed relative to the rotor with origin O' locating on the axis X . The distance from point O to point O' is D_s . At time t_0 , the rotor stays at the location of the dark gray rotor. At time t_1 , the rotor rotates to a new location as the light gray rotor shows. Drawing lessons from radar imaging [22], we consider the total scattering signals from the rotating rotor as a linear superposition of the signals from some main scattering centers. We take one scattering center (*e.g.*, point P in Fig. 3) as an example to illustrate the relative distance change between point P and the transceivers (*i.e.*, Tx and Rx). The rotation radius of P is L_P . When $t = t_0$, scattering center P locates at (x_{t_0}, y_{t_0}) . The angle between $O'P$ and axis X' is φ_0 , and the initial angular speed is Ω_0 . The angle between OP and axis Y is θ_0 . The signal propagation distance $D_p(t_0)$ (green line in Fig. 3) can be divided into two parts: signal transmission distance $D_{OP}(t_0)$ and signal reflection distance $D_{PS}(t_0)$, which can be expressed as Eq. (5):

$$D_P(t_0) = D_{OP}(t_0) + D_{PS}(t_0). \quad (5)$$

These two parts can be further expressed as

$$D_{OP}(t_0) = [D_s^2 + L_P^2 + 2L_P D_s \cos(\varphi_0)]^{\frac{1}{2}}, \quad (6)$$

$$D_{PS}(t_0) = [D_{OP}(t_0)^2 + D_0^2 + 2D_0 D_{OP}(t_0) \cos(\theta_0)]^{\frac{1}{2}}. \quad (7)$$

To further eliminate unknown variables in Eq. (7), we use the sine theorem to analyze triangle $OO'P$:

$$\frac{D_{OP}(t_0)}{\sin(\pi - \varphi_0)} = \frac{L_P}{\sin(\frac{\pi}{2} - \theta_0)}. \quad (8)$$

According to the induction formula, we can further obtain

$$\cos \theta_0 = \frac{L_P \sin \varphi_0}{D_{OP}(t_0)}. \quad (9)$$

Therefore, we put Eq. (9) to Eq. (7), and rewrite Eq. (5):

$$D_P(t_0) = [(D_s + L_P \cos(\varphi_0))^2 + (D_0 + L_P \sin(\varphi_0))^2]^{\frac{1}{2}} \\ + [(D_s + L_P \cos(\varphi_0))^2 + (L_P \sin(\varphi_0))^2]^{\frac{1}{2}}. \quad (10)$$

When $t = t_1$, the rotor rotates to a new location as the light grey rotor shows, and the corresponding scattering center now is point P' , located at (x_{t_1}, y_{t_1}) . The angle between $O'P'$ and axis X' is φ_1 , and the angle between OP' and axis Y is θ_1 . The angle φ_1 at this time can be expressed as Eq. (11):

$$\varphi_1 = \varphi_0 + \Omega_0 \cdot \delta t. \quad (11)$$

Generalizing Eq. (10) and Eq. (11) to common discrete form, we have

$$\varphi_n = \varphi_{n-1} + \Omega_{n-1} \cdot \delta n, \quad (12)$$

$$D_P(n) = [(D_s + L_P \cos(\varphi_n))^2 + (D_0 + L_P \sin(\varphi_n))^2]^{\frac{1}{2}} \\ + [(D_s + L_P \cos(\varphi_n))^2 + (L_P \sin(\varphi_n))^2]^{\frac{1}{2}}. \quad (13)$$

From Eq. (12), we know that the instantaneous period of angular displacement φ_n is decided by the instantaneous angular speed Ω_n . In the measurement, the LoRa node and the rotor are fixed, which means D_0 and D_s in Eq. (13) are constants. Besides, for a given scattering point P , L_P is also constant. Thus, the changes of $D_P(n)$ are completely determined by Ω_n . We can describe this process as

$$D_P(n) = F(\Omega_n). \quad (14)$$

There may be multiple blades on a rotor, and there are multiple scattering points on each blade. The relative distance between the scattering points on the rotor and the transceivers can be expressed as set $D(j)$:

$$D(j) = \{D_1^1(j), D_1^2(j), \dots, D_1^M(j), D_2^1(j), \dots, D_K^M(j)\},$$

where K denotes the number of blades and M denotes the number of scattering points on one blade. For each scattering point on a single blade, the corresponding rotation speed is determined by the same angular speed Ω_n , as described in Eq. (14). For two scattering points located on different blades, the angular displacement difference between them remains a constant value, given by $2\pi \frac{x}{K}$, where x represents the blade order difference. As a result, scattering points on different blades also share the same angular speed Ω_n . Consequently, all elements within the set $D(j)$ are characterized by the same angular speed Ω_n . Since the relative distance we measure is a linear superposition of contributions from all scattering points, we conclude that the angular speed Ω_n is consistent across all scattering points, regardless of their location on the rotor. Note that a rotor of any shape or size can be abstracted into a set of multiple scattering points for modeling purposes. Thus, RoLEX abstracts the rotor into a collection of scattering points and focuses exclusively on their collective rotation, without distinguishing the rotor's shape or size.

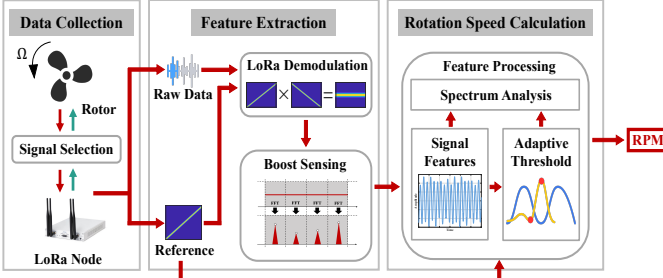


Fig. 4. The Framework of RoLEX

In practice, the model can be directly extended to three-dimensional configurations, *e.g.*, when the rotor lies in a different plane (such as OYZ), by incorporating the corresponding geometric projection of the rotor motion into the distance variation calculation. The underlying physical principle remains unchanged, and the extracted features follow the same periodicity determined by the rotor's angular speed Ω_n . Moreover, although the Tx and Rx are co-located, the impact of self-interference from the direct line-of-sight path is primarily a static component that can be effectively removed by background calibration. Therefore, it does not significantly affect the measurement of rotation speed, as the dynamic variations induced by the rotor dominate the signal changes used for measurement.

Unfortunately, in daily use, we cannot always obtain the exact value of D_0 , D_s , and L_P , because measurement environments may be different. However, instead of identifying individual scattering points, we focus on analyzing the overall changing frequency of all reflected signals. The period of the relative distance variation, as measured, can be used to indirectly derive the rotation speed. Empirically, the phase change of the signal is closely related to the variation in propagation distance. Specifically, when the propagation distance changes by one wavelength, the signal phase undergoes a 2π shift. Although the distance variations caused by multiple scattering points differ, their changing frequencies remain identical (*i.e.*, Ω_n). As a result, after linear superposition, the overall changing frequency remains unaffected. *In RoLEX, we leverage these phase changes as effective signal features and compute their changing frequency to estimate the rotation speed.* Upon receiving the reflected signal, RoLEX processes the LoRa signal to extract the phase sequence as the primary feature for subsequent analysis.

IV. RoLEX DESIGN

In this section, we first give a basic framework of our system, including every component of RoLEX and the workflow. Then, we provide a detailed introduction to the carefully designed main components of RoLEX, highlighting the key mechanisms that enable its robust and accurate performance.

A. RoLEX Framework

In this section, we introduce how we design RoLEX. As shown in Fig. 4, RoLEX consists of three main components.

- **Data collection.** The Data collection module first select the most appropriate signal (*i.e.*, reference signal)

to reduce the interference through the *signal selection* method, and then transmits the LoRa signal for sensing and captures the reflected signal. After that, it outputs the raw data and the reference signal for further processing.

- **Feature extraction.** The Feature extraction module outputs the signal features (*i.e.*, phase changes) based on the analysis in Sec. III-B. The features are extracted through our carefully designed *LoRa Demodulation* sub-module and *Boost Sensing* sub-module.
- **Rotation speed calculation.** The Rotation speed calculation module processes the signal features through our proposed novel *feature processing* method to accurately measure the rotation speed.

In the rest of this section, we introduce these three modules in detail and show how they enable RoLEX to achieve accurate long-distance rotation speed measurement.

B. Data Collection

In this section, we first introduce the main frequency interference faced by RoLEX: the Boundary Frequency. Then, we introduce the proposed novel signal selection method that enables RoLEX to minimize the interference of the Boundary Frequency on the rotation speed measurement.

1) *Boundary Frequency:* We first explain why we should select the appropriate LoRa signal. In Eq. (3), the phase of $H_i(t)$ consists of three parts: $2\pi k\tau_i(t)t$, $2\pi f_c\tau_i(t)$ and $\pi k\tau_i(t)^2$. If the distance between the target and transceivers on i^{th} path is $d_i(t)$, then $\tau_i(t)$ can be calculated as $\tau_i(t) = \frac{2d_i(t)}{c}$. Therefore, the phase of $H_i(t)$ can be expressed as

$$\phi(H_i(t)) = 4\pi k \frac{d_i(t)}{c} t + 4\pi f_c \frac{d_i(t)}{c} - 4\pi k \frac{d_i(t)^2}{c^2}. \quad (15)$$

Note that c is the speed of light, whose value is 3×10^8 m/s. Thus, the third part in Eq. (15) is very small and can be ignored. The equation can be further expressed as

$$\phi(H_i(t)) \approx 4\pi k \frac{d_i(t)}{c} t + 4\pi f_c \frac{d_i(t)}{c} = \phi_1 + \phi_2, \quad (16)$$

where $\phi_1 = 4\pi k \frac{d_i(t)}{c} t$ and $\phi_2 = 4\pi f_c \frac{d_i(t)}{c}$. For the chirp-based LoRa signal, each chirp has a period of T and a time window of t may contain multiple chirps. Thus ϕ_1 can be further represented as

$$\phi_1 = 4\pi k \frac{d_i(t)}{c} (t \% T), \quad (17)$$

where $\%$ means the mod operation.

We can observe that ϕ_1 introduces chirp frequency in the phase, which is an interference, while ϕ_2 represents the phase change caused by the target. We refer to the chirp frequency introduced by ϕ_1 as the Boundary Frequency of LoRa sensing, shown in Fig. 5. Since ϕ_1 and ϕ_2 are mixed in phase, it is difficult to extract the pure features without interference. If the rotation speed of the target is very close to the Boundary Frequency, then the rotation speed will be overridden, resulting in a final calculation error. To reduce the interference of Boundary Frequency, we need to transmit the appropriate LoRa signal for sensing.

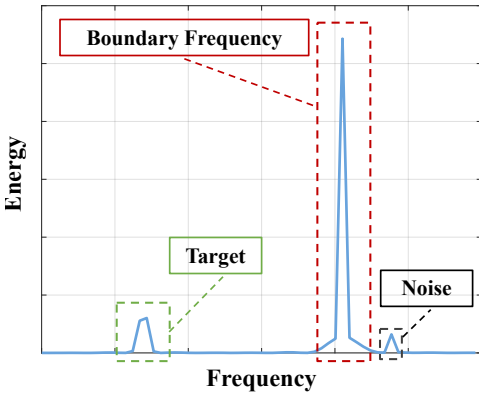


Fig. 5. Example of Boundary Frequency

2) *Signal Selection*: The basic principle of Signal Selection is to ensure that the interference of the Boundary Frequency on the rotation speed measurement can be minimized in the entire frequency domain so that the measurement results can be correct. Fortunately, the Boundary Frequency is a constant and is completely determined by the selected LoRa signal [23]. Given the LoRa signal, we can calculate the Boundary Frequency according to Eq. (18):

$$F_{bf} = \frac{BW}{2^{SF}}, \quad (18)$$

where SF and BW are the Spreading Factor and the Bandwidth of LoRa, respectively. For example, if $SF=12$ and $BW=250\text{ kHz}$, then the Boundary Frequency of LoRa is 61.0351 Hz ($\frac{250\text{ kHz}}{2^{12}} \approx 61.0351$).

To minimize the impact of the Boundary Frequency, we divide the whole speed range into two parts: $Range_1$ ($RS < 40\text{ Hz}$) and $Range_2$ ($RS > 40\text{ Hz}$). Further, we select LoRa signal ($SF=12$, $BW=250\text{ kHz}$) with Boundary Frequency close to 60 Hz (expressed as $LoRa_60$) to measure the target in $Range_1$ and select LoRa signal ($SF=12$, $BW=125\text{ kHz}$) with Boundary Frequency close to 30 Hz (expressed as $LoRa_30$) to measure the target in $Range_2$. The purpose of this approach is to ensure that the Boundary Frequencies do not appear in the corresponding range.

Note that other LoRa signals with higher Boundary Frequencies (e.g., $BW=500\text{ kHz}$) can also be used in RoLEX, since the aliasing peaks can be suppressed via low-pass filtering. However, the Boundary Frequency of a LoRa signal is determined by its symbol duration T , which is calculated as $T = \frac{2^{SF}}{BW}$. The corresponding Boundary Frequency is $F_{bf} = \frac{1}{T}$. Thus, higher Boundary Frequency leads to shorter LoRa symbol durations. While this increases time resolution, it also degrades frequency resolution and makes it more difficult to distinguish fine-grained frequency peaks. Moreover, shorter chirp durations increase the system's sensitivity to noise and multipath, reducing the robustness of feature extraction. Therefore, we adopt LoRa signals with the smallest Boundary Frequencies ($LoRa_30$ and $LoRa_60$), which offer a good balance between spectral resolution, robustness, and applicability across a wide speed range.

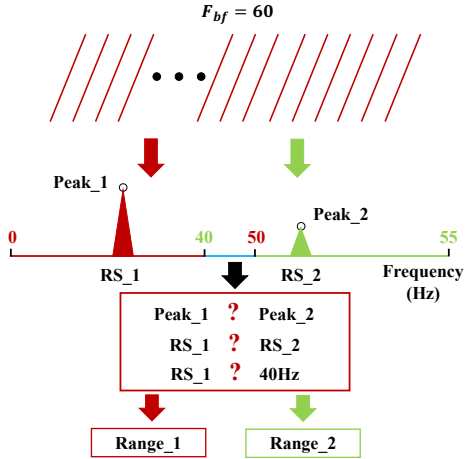


Fig. 6. Initial Classification

Algorithm 1: Initial Classification

Input: Classification Signal $LoRa_class$.
Output: Speed Range R .

```

1 Peak_class1 ← peak_Range_1(LoRa_class);
2 Peak_class2 ← peak_Range_2(LoRa_class);
3 RS_class1 ← RS_Range_1(LoRa_class);
4 RS_class2 ← RS_Range_2(LoRa_class);
5 if Peak_class1 is much greater than Peak_class2
   and RS_class1 < 40 Hz then
6   | R ← Range_1;
7 else
8   | if RS_class2 is the harmonic of RS_class1 and
      RS_class1 < 40 Hz then
9     | | R ← Range_1;
10  | else
11    | | R ← Range_2;
12  | end
13 end
14 return R.

```

Based on the design above, in $Range_1$, the Boundary Frequency will not interfere with the measurement of rotation speed because it is already filtered out by the band-pass filter. However, in $Range_2$, $LoRa_30$ will produce a harmonic interference close to 60 Hz , which will affect the measuring result when the rotation speed is nearly 60 Hz . To solve this problem, we propose a novel Feature Processing method, which will be introduced in detail in Sec. IV-D. Please note that the reason why we use $LoRa_30$ for $Range_2$ is because the harmonic frequency of $LoRa_30$ is much smaller than the Boundary Frequency of $LoRa_60$, which results in better differentiation of target and interference in the frequency domain. In this way, we can reduce the interference and ensure the accuracy of measurements.

If the rated rotation speed is known, we can directly select the corresponding LoRa signal and use it to verify the rated speed. When facing an unknown target, we can first perform an initial classification of the target to determine which LoRa signal we should transmit. The process of initial classification is shown in Alg. 1.

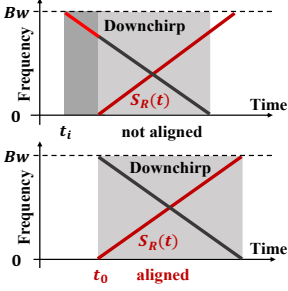


Fig. 7. Signal Alignment

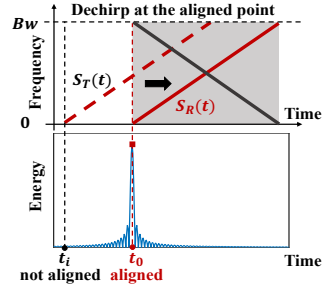
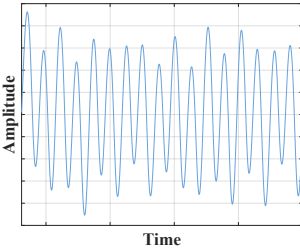
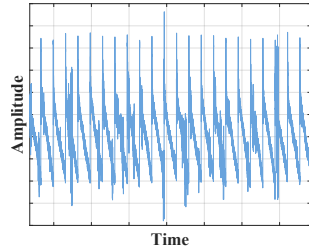


Fig. 8. LoRa Dechirp



(a) Features from Boost Sensing



(b) Features from Raw Dechirp

Fig. 9. Visualization of Signal Features

Firstly, as shown in Fig. 6, we transmit *LoRa_60* as the classification signal and collect the signal reflected by the target. Then, we follow the complete workflow of RoLEX to extract the rotation features in two ranges, respectively, and calculate the frequency domain peak and rotation speed (line 1 - 4). Specifically, we extract the peak values and calculate the results in the two ranges, frequency below 50 Hz and frequency from 40 Hz to 55 Hz, respectively. We designate the frequency range from 40 Hz to 50 Hz as a buffer band to account for potential system failure in detecting the boundary (40 Hz) during initial classification.

Secondly, after extracting the peak values and calculating the results, we need to determine which speed range the current rotation speed should be in. This is based on a very important assumption: *the frequency energy caused by rotation is greater than the frequency energy of the noise*. Because we only need to classify two ranges, we need to determine whether the result extracted in *Range_1* is the change caused by the target. This can be divided into two cases. The first case is if the peak value in *Range_1* is greater than the peak value in *Range_2*, and *RS* in *Range_1* is lower than 40 Hz (line 5), then the system will classify the target into *Range_1*. The second case is that the selected peaks in the two ranges are harmonics of each other. Harmonic detection is performed by evaluating both the frequency ratio and the energy ratio between two frequencies. Specifically, we consider one frequency to be a harmonic of the other if the following two conditions are satisfied: (1) their frequency ratio is close to 2, *i.e.*, $|RS_{class2}/RS_{class1} - n| < \delta_f$, where we set $n = 0.2$ and $\delta_f = 2$; (2) the energy ratio between the two frequencies exceeds a threshold, *i.e.*, $Peak_{class2}/Peak_{class1} > \theta$, where we set $\theta = 0.4$. This dual-criteria check ensures reliable identification of harmonic relationships. In this case, if *RS* in *Range_1* is lower than 40 Hz (line 8), then the system will also classify the target into *Range_1*. If neither of the above two cases is satisfied, it means that *RS* is either between

Algorithm 2: LoRa Demodulation

Input: Received Signal $S_R(t)$, Baseband Upchirp S_{up} and Baseband Downchirp S_{down} .

Output: Dechirp Signal $S_{dechirp}$.

```

1  $S_{dechirp}(t) \leftarrow \emptyset;$ 
2  $S_{xcorr}(t) \leftarrow xcorr(S_R(t), S_{up});$ 
3  $\{peaks_k\}_{k \in [K]} \leftarrow findpeaks(S_{xcorr}(t));$ 
4  $\{S_{symbol_n}\}_{n \in [N]} \leftarrow split(S_R(t), \{peaks_k\}_{k \in [K]});$ 
5 for  $n \in [N]$  do
6   |  $Join(S_{dechirp}, S_{symbol_n} * S_{down});$ 
7 end
8 return  $S_{dechirp}.$ 
```

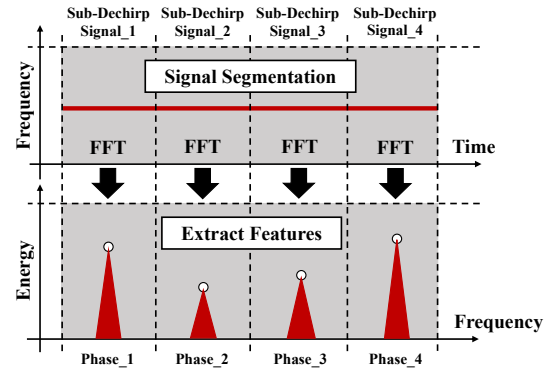


Fig. 10. Example of Boost Sensing

50 Hz and 55 Hz, or above 55 Hz. Then the system will classify the target into *Range_2*. Based on the classification results, RoLEX will transmit the corresponding signal for sensing.

C. Feature Extraction

In this section, we introduce the two sub-modules (*i.e.*, LoRa Demodulation and Boosting Sensing) in detail and show how RoLEX achieves long-distance measurement.

1) *LoRa Demodulation*: After Signal Selection, RoLEX transmits the corresponding LoRa signal and captures the signal reflected by the target. To reduce the impact of long-distance signal attenuation, RoLEX first performs LoRa demodulation on the received signal to improve the Signal-to-Noise Ratio (SNR). The process of LoRa demodulation is shown in Alg. 2.

Firstly, we need to align the signals and accurately extract each LoRa symbol for subsequent demodulation. If we do not perform signal alignment, as shown in Fig. 7, the red part of the downchirp in the dark gray area will not only retain the effects of the CSS modulation, but also introduce new frequency interference, thereby affecting the signal feature extraction. However, after signal alignment, the influence of CSS will be completely eliminated and the system will extract pure signal features, shown in Fig. 7. Since the signal we transmit is the baseband upchirp with no frequency offset components, we use the same upchirp as the reference signal to perform alignment. We perform a cross-correlation operation between the received signal and the reference signal (line 2). As illustrated in Fig. 8, when the reference signal is aligned with the received signal, the cross-correlation will produce

Algorithm 3: Boost Sensing

Input: Dechirp Signal in Time Window $S_{dechirp}(t)$,
Number of Segments N , Dechirp Length T .

Output: Signal Features S_F .

```

1  $S_F \leftarrow \emptyset;$ 
2  $\{S_{one dechirp_k}\}_{k \in [K]} \leftarrow split(S_{dechirp}(t), T);$ 
3 for  $k \in [K]$  do
4    $\{Sub\_dechirp_n\}_{n \in [N]} \leftarrow seg(S_{one dechirp_k});$ 
5   for  $n \in [N]$  do
6      $S_{FFT} \leftarrow FFT(Sub\_dechirp_n);$ 
7      $S_{peak} \leftarrow find\_maxpeak(S_{FFT});$ 
8      $Join(S_F, phase(S_{peak}));$ 
9   end
10 end
11 return  $S_F.$ 
```

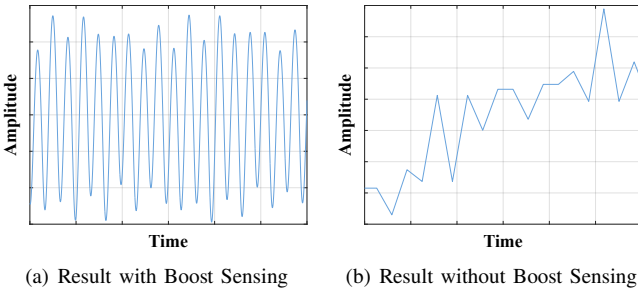


Fig. 11. Results of Verification Experiment

a peak whose abscissa represents the first sampling point position of one received LoRa symbol. This alignment ensures that the time-domain synchronization is accurately established, enabling consistent extraction of signal features.

Because the speed of light is extremely high, the relative time differences among multipath signals are negligible. Consequently, they arrive at the LoRa node almost simultaneously, and the cross-correlation peak can reliably mark the symbol start position. This eliminates the need to distinguish individual paths and simplifies alignment while maintaining robustness in diverse environments.

Secondly, RoLEX tracks the position of each peak and divides the received signal into independent LoRa symbols according to the symbol length (line 3 - 4). For each LoRa symbol in the received signal, RoLEX performs dechirp (line 6), which is achieved by multiplication of the LoRa symbol with the predefined baseband downchirp, described in Sec. II-A. Since each LoRa symbol is aligned, the quadratic component that changes over time in the signal phase can be completely eliminated. Meanwhile, the signal energy within the entire frequency domain bandwidth can be concentrated on a specific frequency, which solves the problem of low SNR and provides a stable signal for processing. The dechirp signal will be further processed in subsequent modules to extract signal features and calculate the rotation speed.

2) *Boost Sensing*: Traditional LoRa sensing methods cannot realize the sensing of high-frequency motions [13], because the sampling rates of the extracted signal features do not satisfy the Nyquist sampling law. A simple solution to

increase the sampling rates is reducing the spreading factor (SF) or increasing the bandwidth (BW) of the LoRa signal. However, this requires dedicated LoRa chips that can adjust the corresponding parameters. Meanwhile, directly extracting phase information from the raw dechirp signal [18] will also introduce a lot of noise in the signal features. As shown in Fig. 9(b), the features directly obtained from raw dechirp signal are heavily corrupted by noise, making it difficult to identify meaningful patterns. This is because raw phase extraction is highly sensitive to additive noise and multipath, where even small amplitude fluctuations can induce large random phase shifts. To enable accurate rotation speed estimation, it is therefore crucial to eliminate such interference and extract clean, reliable signal features.

We observe that the dechirp signal exhibits continuity, meaning that each sampling point contains both the rotational information of the target and noise components. This observation enables us to exploit the continuous nature of the signal to simultaneously increase sampling rates and reduce noise interference during feature extraction, regardless of the specific LoRa signal used. Thus, we propose a Boost Sensing method for RoLEX, as detailed in Alg. 3.

Firstly, RoLEX accumulates dechirp signals for a given time window length. Then, RoLEX divides the signal in the window according to the length of the upchirp to obtain a set of dechirp sequences for each LoRa symbol (line 2).

Secondly, as illustrated in Fig. 10, RoLEX divides each dechirp sequence into multiple segments in order to improve the sensing sampling rates (line 4). We suppose that a LoRa dechirp is divided into N segments. Now, the sensing sampling rates will be N times than before, expressed as Eq. (19):

$$F_{sensing} = F_{bf} * N. \quad (19)$$

Finally, RoLEX performs the FFT on each segment and extracts the phase of the maximum peak (line 6 - 8). Note that what we extract is the phase information of the frequency domain peak, not the initial phase of each segment. This is because the phase of the frequency domain peak is equal to the initial phase of the maximum frequency energy component signal in this segment. This method will ensure that the noise in the features can be suppressed to the greatest extent. As shown in Fig. 9(a), our Boost Sensing method produces clean and distinct signal features, which are more suitable for accurate rotation speed measurement.

Then, we discuss the selection of the signal segment parameter N , which determines the trade-off between the sensing accuracy and the rotation speed that RoLEX can measure. According to Eq. (19), any value of N that ensures $F_{sensing}$ satisfies the Nyquist sampling theorem is theoretically sufficient for accurate measurement. A larger N allows RoLEX to sense higher rotation speeds but reduces the length of each signal segment, potentially lowering the estimation accuracy of the FFT due to insufficient frequency resolution. Since the product of N and the segment length equals the length of one transmitted LoRa chirp, RoLEX selects $N = \sqrt{L_{dechirp}}$, where $L_{dechirp}$ is the length of one LoRa dechirp, to achieve a balance between these two factors.

Algorithm 4: Rotation Speed Calculation

Input: Signal Features S_F , Time Window W , Overlap Ratio O_r and Selected Signal L .

Output: Rotation Speed RS .

```

1  $RS \leftarrow \emptyset;$ 
2  $\{S_{Fn}\}_{n \in [N]} \leftarrow sliding(S_F, W, O_r);$ 
3 for  $n \in [N]$  do
4    $RS\_Spec \leftarrow Spectrum(S_{Fn});$ 
5    $peaks\_en \leftarrow peaks(RS\_Spec);$ 
6   if  $L == LoRa\_60$  then
7     if  $Exist\_Harmonic(peaks\_en)$  then
8        $Join(RS, fundamental(peaks\_en));$ 
9     else
10       $Join(RS, max(peaks\_en));$ 
11    end
12  else
13    if  $length(peaks\_en) \geq 2$  then
14       $\tau \leftarrow threshold(max(peaks\_en), noise);$ 
15       $ratio \leftarrow$ 
16       $max(peaks\_en)/sec(peaks\_en);$ 
17      if  $ratio < \tau$  then
18         $Join(RS, sec(peaks\_en));$ 
19      else
20         $Join(RS, max(peaks\_en));$ 
21      end
22    else
23       $Join(RS, max(peaks\_en));$ 
24    end
25  end
26 return  $RS.$ 
```

Further, we explore the theoretical sensing upper limit of RoLEX. In our system, when RoLEX utilizes *LoRa_30* for measurement with a LoRa node's ADC sampling rate of 1 MHz [23], $F_{sensing}$ can reach an impressive 5430 Hz, as derived from Eq. (19). This capability allows RoLEX to measure rotation speeds exceeding 100 000 RPM, meeting the requirements of high-speed industrial machinery monitoring [24], [25]. Such performance not only demonstrates the scalability of RoLEX in handling high-speed sensing tasks but also highlights its potential to expand the application boundaries of wireless sensing systems in demanding industrial scenarios.

We also employ an example to demonstrate the effectiveness of our proposed method. The rotation frequency of the target is about 40 Hz, and we use *LoRa_60* for experiments. After obtaining the reflected signal, we use the workflow of RoLEX and the non-segmentation method to extract signal features, respectively. The results are shown in Fig. 11. We observed that the signal features using the workflow of RoLEX (Fig. 11(a)) show obvious stable periodicity. On the contrary, the signal features using the non-segmentation method (Fig. 11(b)) do not show periodicity, and the signal noise has a stronger impact on the results. What's more, the signal features extracted by the non-segmentation method do not satisfy the Nyquist sampling law ($61 \text{ Hz} < 80 \text{ Hz}$), which means the features do not contain

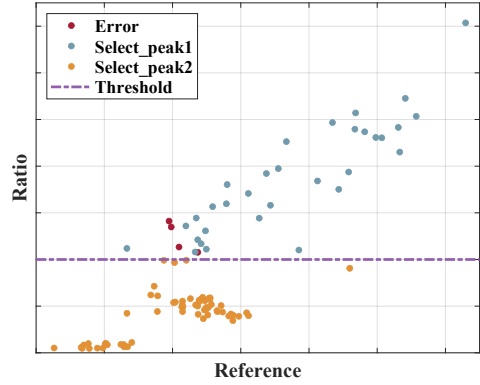


Fig. 12. Example of Threshold

enough information. Thus, this example demonstrates that the Boosting Sensing method can solve the problem of high-frequency motion sensing with LoRa signal.

D. Rotation Speed Calculation

In this section, we introduce the proposed novel feature processing method with an adaptive threshold design that enables RoLEX to measure the rotation speed accurately, which is shown in Alg. 4.

Firstly, RoLEX applies proportionally overlapping sliding windows to segment the signal features within each time window, and then performs spectrum analysis on each segment (lines 2 - 5). Since each scattering point on the rotor is controlled by the same angular velocity according to the analysis in Sec. III-B and we have implemented signal alignment introduced in Sec. IV-C1, there are only three frequencies that may exist in the signal spectrum, *i.e.*, the rotation speed, the Boundary Frequency, and the Harmonic Frequency (harmonic components of the rotation speed or the Boundary Frequency). Then, RoLEX will use our proposed novel feature processing method to accurately determine which frequency represents the true rotation speed.

Secondly, if it is in *Range_1* ($RS < 40 \text{ Hz}$), since the Boundary Frequency has been filtered out, RoLEX only needs to determine whether Harmonic Frequency exists. If it exists, RoLEX will select the peak of the baseband frequency as the result. Otherwise, the peak with the highest energy in the spectrum will be selected (line 6 - 11).

Thirdly, if it is in *Range_2* ($RS > 40 \text{ Hz}$), due to the high rotation speed of the target, the Harmonic Frequency of the rotation speed will disappear after filtering, but the Boundary Frequency's harmonic component of *LoRa_30* will become the main interference. RoLEX needs to determine which frequency represents the rotation speed. We achieve this by designing a novel adaptive threshold. Specifically, if RoLEX detects more than two peaks in the spectrum, it means that both the rotation speed and the Boundary Frequency exist and they do not coincide. To obtain the rotation speed, we calculate the ratio of the highest peak and the noise and further calculate the difference in magnitude m . Then we calculate the threshold τ (line 14) according to Eq. (20):

$$\tau = m \cdot 10^m. \quad (20)$$

Next, RoLEX will compare the relationship between the ratio of the highest and the second peak and the threshold

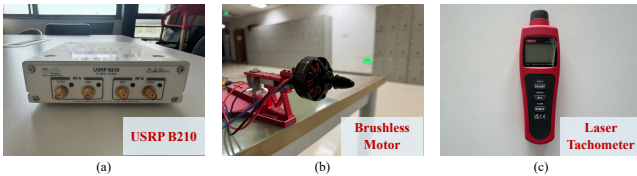


Fig. 13. Equipment Used in Experiments

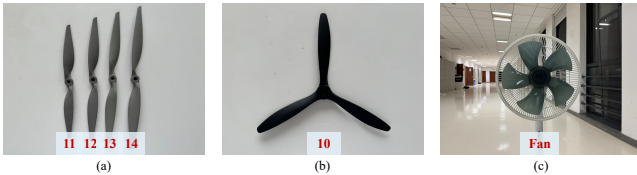


Fig. 14. Different Rotating Objects

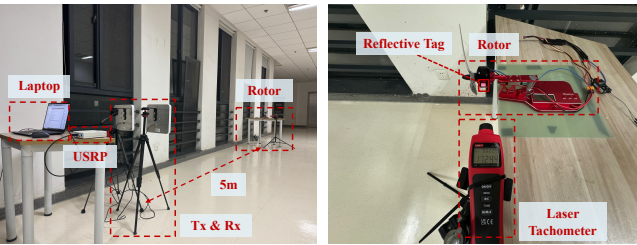


Fig. 15. Experimental Testbed

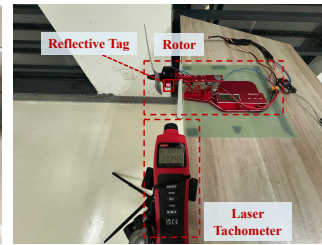


Fig. 16. Scenario on the Rotor Side

(line 15). If the ratio is less than the threshold, it means there are other high-energy frequency peaks in the spectrum, *i.e.*, rotation speed. Then, RoLEX will select the second peak as the calculation result. Otherwise, it means that the energy of the second peak is not much different from the noise and only one valid peak exists in the spectrum, then RoLEX will select the valid peak as the calculation result (line 16 - 20). If only one peak is detected, it means that the rotation speed and the Boundary Frequency coincide at this time, so RoLEX will select this maximum peak as the calculation result (line 22).

We further test a rotor with a diameter of 30 cm and width of 2.8 cm at a distance of 1 m to 15 m to evaluate the rationality of our proposed threshold design. As shown in Fig. 12, among the 100 sets of data we collected, only four sets of data have errors (*i.e.*, red dots in Fig. 12), and they are all results when the distance is 15 m. Since the rotor area is small, the energy of the reflected signal may be contaminated by noise over long distances. In real life, the tested target is usually larger than the rotor we use, and the distance is usually less than 10 m. Thus, our threshold design is reasonable and can be further generalized to longer distances and larger targets.

Finally, RoLEX tracks the selected peak within the spectrum of each feature segment and uses it as the measurement of the rotation speed for the current time. Moreover, when it detects that the rotation speed is at the boundary of the two speed ranges, RoLEX can automatically switch the transmitted signal to achieve cross-range measurement.

V. EVALUATION

A. Implementation and Experimental Setup

We build a prototype of RoLEX using a USRP B210 and a brushless motor, which can rotate in both ranges (Fig. 13). We set the central frequency as 915 MHz and employ UHD and GNU-Radio library [26] to generate the LoRa signals we

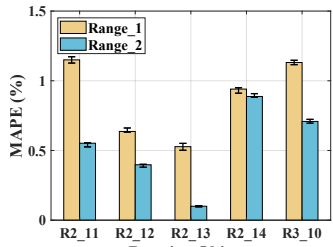


Fig. 17. RoLEX vs. Different Rotating Objects

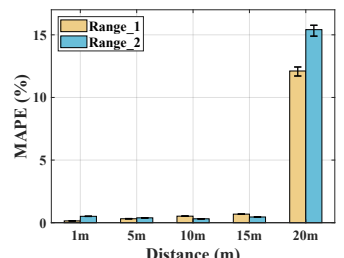


Fig. 18. RoLEX vs. Different Distances with a Rotor



Fig. 19. Scenario of Distance Experiment with a Fan

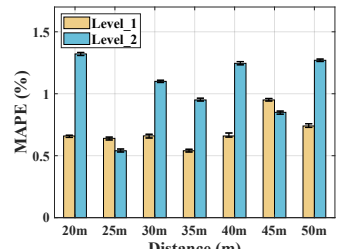


Fig. 20. RoLEX vs. Different Distances with a Fan

need. USRP B210 will then collect the LoRa signal samples reflected by the target at a sampling rate of 1 MHz and transmit the data back to the PC. We implement the proposed methods in Matlab and all the processing happens on a Laptop with Intel Core i7-1260P processor and 16 GB memory.

To better evaluate the performance of RoLEX, we prepare rotors of different shapes and sizes (Fig. 14), where the number indicates the length of one blade. If a rotor has two blades and its diameter length is 11 inches, then we call it *R2_11*. Moreover, we also prepare an electric fan for evaluation, shown in Fig. 14. The setup of the experimental testbed is shown in Fig. 15. Unless otherwise specified, the default rotor we use is *R2_13*, and the test distance is 5 m. The signals used in the experiments are *LoRa_60* ($SF = 12$, $BW = 250$ kHz) and *LoRa_30* ($SF = 12$, $BW = 125$ kHz). The default computational parameter N (analyzed in Sec. IV-C2) is set to 128 for *LoRa_60*. Since *LoRa_30* is twice as long as *LoRa_60*, and its chirp length is not a perfect square, we adopt $N = 256$ as the default for *LoRa_30*. We use a default window overlap ratio of 50% throughout the experiments.

The ground truth of the brushless motor and the fan is obtained by a commercial laser tachometer UNIT UT372 [27] (Fig. 13). As shown in Fig. 16, the reflective tag is attached to the motor, and the tachometer is fixed next to the tag. Therefore, the measurement of ground truth and the measurement of RoLEX are carried out simultaneously. In this paper, we use the Mean Absolute Percentage Error (MAPE) [4] between the measurement result and the ground truth as the metric.

B. Evaluation of Measuring Fixed Rotation Speed

In this section, we conduct a comprehensive evaluation of RoLEX's performance in measuring fixed rotation speeds. First, we evaluate the performance on different rotating objects, different measurement distances, different rotation speeds and different measurement angles. Then, we evaluate the robustness and through-wall measurement performance.

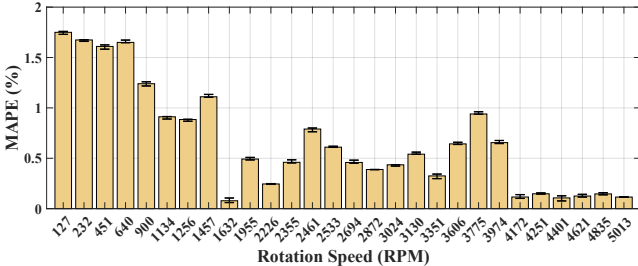


Fig. 21. RoLEX vs. Different Rotation Speeds

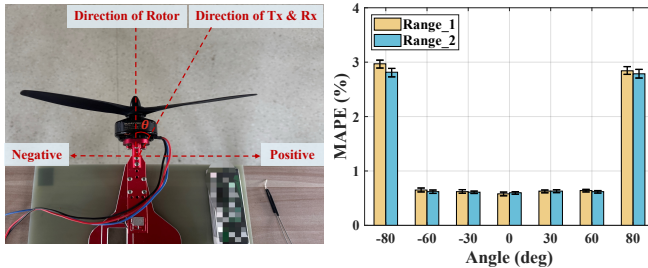


Fig. 22. Scenario of Different Angles

1) *Impact of Different Rotating Objects:* To evaluate the accuracy of RoLEX measuring different rotating objects, we test the measurement performance of RoLEX with five different rotors. We control the brushless motor to rotate in two ranges, and for each rotor, we collect 5 sets of rotation data in each range and then calculate the MAPE. The experimental results are shown in Fig. 17. The average measurement error of RoLEX is less than 0.7% and the maximum error is less than 1.2% with different rotors. For a rotor with two blades, theoretically, the larger the rotor, the better the performance should be. However, for the brushless motor we use, *R2_14* will deflect when rotating due to its large size. Additionally, all the rotors we use will experience slight displacements during rotation. Both of these situations may affect the measurement results. But even so, the measurement error is still less than 1%. Thus, we can conclude that RoLEX can stably measure rotating objects of different shapes and sizes with an average measurement error less than 0.7%.

2) *Impact of Measurement Distance:* The measurement distance is of great importance for the safety of the operators. We evaluate the impact of the measurement distance on RoLEX. First, we conduct experiments using the rotor. Here, we use *R2_13* for experiments, and the measurement distance increases from 1 m to 20 m with a step size of 5 m. We conduct experiments on both two ranges and the results are shown in Fig. 18. When the measurement distance is less than or equal to 15 m, the measurement error of RoLEX in both two ranges is less than 0.8%. However, when the measurement distance is increased to 20 m, the measurement error in both two ranges increases to more than 12%. We analyze that this may be caused by the reflected signal being too weak. For a measurement distance of 20 m, the dimensions of a 13-inch rotor are small, so the reflected signal is weak and may be below the noise floor. Even if RoLEX concentrates the energy of the reflected signal in advance, in this scenario, it is still difficult for RoLEX to separate the energy of the signal features from the noise floor. However, in daily use, the size of the target is usually larger than the rotor we use, and the measurement distance does not exceed 10 m.

To further explore the potential of RoLEX in long-distance measurement, we replace the rotor with a fan (shown in Fig 14) and conduct experiments. The setup of the experimental scene is shown in Fig. 19. We increase the measurement distance starting from 20 m and test the fan at two rotation speeds (*Level_1* and *Level_2*). The ground truth is measured in advance using the laser tachometer, and the result is shown in Fig. 20. Since the reflected energy of the fan blades is stronger than that of the rotor, the measurement distance of RoLEX has been further improved. Even at a distance of 50 m, RoLEX can still ensure the measurement error less than 1.3%. Please note that the longest distance of the corridor selected in our experimental scenario is 50 m, which indicates that the measurement limit of RoLEX will be higher than 50 m. In actual use, the measurement distance of 50 m is enough to meet the safety measurement task. Therefore, we conclude that RoLEX can complete ultra-long-distance measurement tasks and ensure the measurement error less than 1.3%.

3) *Impact of Different Rotation Speeds:* We evaluate the measurement performance of RoLEX for different rotation speeds. We control the rotation speed of the motor from 100 RPM to 5100 RPM and measure it using RoLEX. The results are shown in Fig. 21. Overall, RoLEX can achieve rotation speed measurement in the range of 100 RPM to 5100 RPM with an average measurement error less than 0.69% and maximum measurement error less than 1.75%. From the results, we can observe that the measurement error at low rotation speed is larger than the measurement error at high rotation speed. This is because, at low rotation speed, a deviation of just one sampling point can lead to very high errors. However, RoLEX can still achieve a measurement error less than 1.75% in low-speed measurement, which fully demonstrates the effectiveness of RoLEX. Meanwhile, we also observe that the error increases when the rotation speed approaches 3600 RPM. This is because 3600 RPM is close to the Boundary Frequency. Therefore, RoLEX needs to carefully select the peak of the spectrum for measurement at this time. Experimental results show that when the rotation speed is close to the Boundary Frequency, the measurement error of RoLEX is always less than 1%, which shows that the signal feature processing mode we propose for RoLEX is effective.

Note that 5100 RPM is not the measurement limit of RoLEX. According to the analysis in Sec. IV-C2, RoLEX can theoretically measure rotation speed exceeding 100 000 RPM. In industrial production and our daily life, machines with rotating parts can be divided into three ranges according to their rotation speed: low, medium, and high rotation speed range. Geared motor [28] is a common low-rotation speed object, and the rotation speed is usually less than 500 RPM. In the medium rotation speed range, common ones include rotor bearing systems [29], fans, and most common rotating objects in life, whose rotation speed ranges from about 1500 RPM to 3000 RPM. Machines in the high rotation speed range typically have rotation speeds above 3000 RPM, for example, aircraft generators [24] and vehicle-mounted generators [25]. But even for aircraft generators [24], their rated rotation speed is just around 5000 RPM. Components that rotate at higher speeds are often enclosed within the

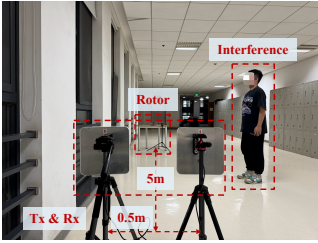


Fig. 24. Scenario of Interference Experiment

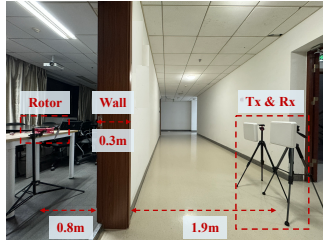


Fig. 25. Scenario of Obstruction Experiment

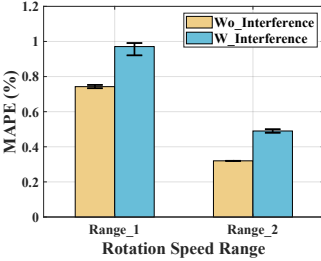


Fig. 26. RoLEX vs. Interference

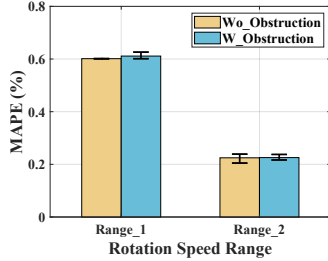


Fig. 27. RoLEX vs. Obstructions

machine and cannot be measured from the outside. Thus, the measurement capability of up to 5000 RPM can complete most of the measurement tasks in both industrial and daily life scenarios. While RoLEX theoretically supports rotation speeds exceeding 100 000 RPM, we acknowledge that in real-world deployments, factors such as hardware limitations and channel noise may degrade measurement accuracy at ultra-high speeds. Investigating these effects remains an important direction for our future work.

4) Impact of Different Measurement Angles: To evaluate the robustness of RoLEX under varying measurement angles, we design the experimental scenario illustrated in the Fig. 22. The measurement angle θ is defined as the angle between the incident signal direction (*i.e.*, Tx & Rx) and the rotor's orientation. When the transceivers are positioned to the right of the rotor, θ is considered positive; otherwise, it is negative. The measurement angles are symmetrically adjusted along the positive and negative axes, ranging from -80 degrees to 80 degrees. The results, presented in Fig. 23, demonstrate the robustness of RoLEX across all tested angles. For measurement angles between -60 degrees and 60 degrees, the Mean Absolute Percentage Error (MAPE) remains consistently low, below 0.75% . Even at extreme angles of -80 degrees and 80 degrees, the MAPE increases slightly but remains under 3% . By maintaining high accuracy across a wide range of angles, RoLEX demonstrates its robustness and adaptability in real-world scenarios, ensuring reliable measurements even in non-ideal configurations.

5) Impact of Environmental Interference: To evaluate the robustness of RoLEX to environmental interference, a human volunteer is asked to step near the RoLEX system to create slight interference, shown in Fig. 24. We compare the results with and without environmental interference while the measurement distance is 5 m . As shown in Fig. 26, slight environmental interference has almost no effect on RoLEX. The measurement error in *Range_1* only increased by 0.2% , while that in *Range_2* is 0.17% . The measurement error of RoLEX is less than 1% regardless of whether there is

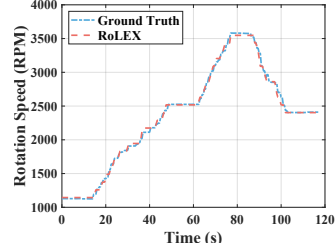


Fig. 28. Rotation Speed Tracking Results (Range_1 to Range_2)

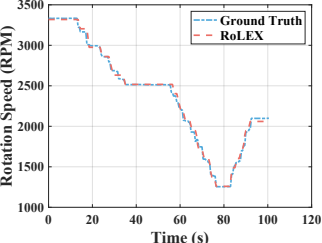


Fig. 29. Rotation Speed Tracking Results (Range_2 to Range_1)

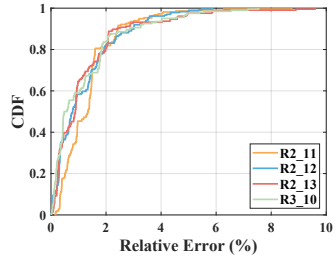


Fig. 30. CDF of Tracking Results

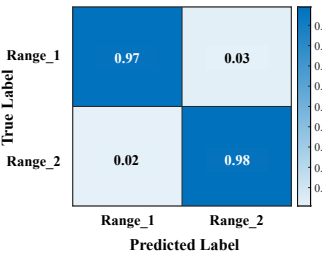


Fig. 31. Results of Classification

environmental interference or not. We analyze that this may be because RoLEX focuses on high-frequency periodic motion rather than low-frequency motion.

It is also worth noting that slight displacements of the rotors during rotation, an inherent aspect of the setup, do not compromise measurement accuracy. RoLEX consistently achieved an average error below 1% , further underscoring its robustness against minor environmental disturbances.

6) Impact of Obstructions: Since LoRa signals have good through-wall communication performance, we further evaluate the through-wall measurement capabilities of RoLEX, shown in Fig. 25. The thickness of the wall is 0.3 m , and the measurement distance is 3 m . We perform experiments in both two rotation speed ranges.

The results, shown in Fig. 27, demonstrate that obstructions have a negligible impact on the system's accuracy. The overall measurement error of RoLEX remains consistently below 0.62% , even in the presence of walls. Specifically, the measurement error in both two ranges increases by less than 0.01% when obstructions are introduced, compared to the error observed in unobstructed conditions. Since we have concentrated the energy of the reflected signal in advance (*i.e.*, effect of LoRa Demodulation and Boost Sensing on reflected signals), the ability of RoLEX for through-wall measurement is guaranteed. Therefore, we can conclude that RoLEX can complete the through-wall measurement task with a measurement error less than 0.62% .

C. Evaluation of Tracking Variable Rotation Speeds

In this section, we evaluate the performance of RoLEX in tracking variable rotation speeds. Since RoLEX can automatically switch transmission signals and signal processing modes to adapt to different rotation ranges, we test the tracking performance on four different rotors. We control the rotation speed of the motor to continuously change within two ranges, and use the laser tachometer to collect the ground truth. For each rotor, we collect 5 sets of data and finally calculate their

TABLE I
COMPUTATIONAL OVERHEAD OF RoLEX

	Demodulation	Boost Sensing	Calculation
Time (s)	0.351 s	0.092 s	0.109 s
Memory (MB)	63.58 MB		

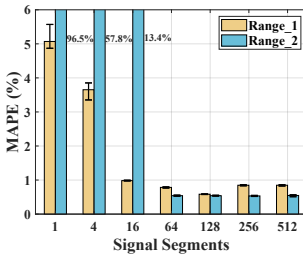


Fig. 32. RoLEX vs. Segments

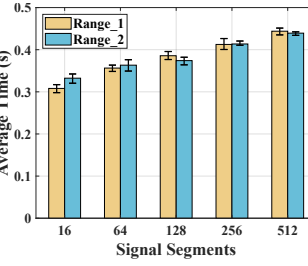


Fig. 33. Computation Time

average error. Tracking results across two ranges are shown in Fig. 28 and Fig. 29. It can be seen from the results that RoLEX can achieve the tracking of the rotation speed very well, whether it is increasing from a low rotation speed or decreasing from a high rotation speed. At the boundary of the two ranges, RoLEX can well identify the range boundary and switch the signal as well as processing mode to achieve cross-range rotation speed tracking.

We further calculate the error distribution for four different rotors, shown in Fig. 30. From the CDF plot, we know that the relative error is roughly the same with four different rotors, which fully demonstrates that RoLEX is robust to different rotors. Overall, the relative tracking error is less than 2% in 80% of cases and less than 2.8% in 90% of cases for every rotor. Even though the signal energy reflected by $R2_11$ is smaller than that of $R2_13$, the median error of their tracking results only differs by 0.5%. Therefore, we can conclude that RoLEX is able to achieve rotation speed tracking of different objects with relative error less than 2% in 80% of cases and less than 2.8% in 90% of cases.

D. Evaluation of Computational Overhead of RoLEX

To evaluate the computational overhead of RoLEX, we measure the time and memory consumption of a single measurement, which includes three primary processing stages: signal demodulation, boost sensing, and final rotation speed calculation. As shown in Tab. I, the average processing time for one measurement is approximately 0.552 s on a standard laptop equipped with an Intel Core i7-1260P processor and 16 GB RAM. Among the three stages, demodulation takes the majority of the time (0.351 s), followed by calculation (0.109 s), and boosted sensing is relatively lightweight (0.090 s). The peak memory consumption during the process is 63.58 MB. Note that we do not apply aggressive optimizations in our MATLAB implementation and we will discuss potential strategies for further improvement in Sec. VII-B. Nevertheless, these results indicate that RoLEX remains computationally lightweight, achieving sub-second latency with low memory usage.

E. Evaluation of Key Design Choices in RoLEX

In this section, we evaluate the performance of three key design choices in RoLEX: Signal Selection, Boost Sensing and the Overlapping Sliding Window. For the Signal Selection

evaluation part, we mainly evaluate the performance of the initial classification to evaluate whether RoLEX can select the correct transmission signal. For the Boost Sensing evaluation part, we first evaluate the impact of different signal segments on RoLEX performance. Then, we evaluate the impact of different signal segments on the computation time of RoLEX. For the Overlapping Sliding Window evaluation part, we evaluate whether overlapping segments can enhance the system's sensitivity and robustness in dynamic rotation tracking.

1) *Initial Classification*: To evaluate the effectiveness of initial classification, we collect a total of 200 sets of rotation data with different rotors in two rotation ranges, with the measurement distance within 10 m. Among them, there are 100 sets of data for *Range_1* and 100 sets of data for *Range_2*. Then, we classify these data using the initial classification module of RoLEX, and the results are shown in Fig. 31. Experimental results demonstrate that RoLEX achieves high performance in classification tasks. Across both data classification ranges, RoLEX attains an accuracy exceeding 97%. Specifically, the classification accuracy reaches 97% in the *Range_1* experiment and 98% in the *Range_2* experiment. It is worth noting that RoLEX requires only 1 second of rotational data to accurately classify the target's rotation speed, which is highly practical for everyday applications. These results confirm the effectiveness of RoLEX's initial classification module, providing a reliable foundation for subsequent rotation measurement and tracking tasks.

2) *Boost Sensing*: We first evaluate the impact of different signal segments on the measurement results. We select data with rotation speed 1632 RPM for *Range_1* and data with rotation speed 3130 RPM for *Range_2*. Then, we calculate the MAPE for different signal segments. The results are shown in Fig. 32. In *Range_1*, if we do not use the Boost Sensing method, the measurement error is higher than 5%. This is because, according to the Nyquist sampling law, LoRa_60 can measure rotation speed below 1800 RPM. If the rotation speed of the data we choose is 1955 RPM, the error will increase to 30%. As the signal segmentation increases, the measurement error of RoLEX will gradually decrease. This shows that the increase in the sensing sampling rate helps RoLEX detect high-frequency motion targets. In *Range_2*, if we do not use the Boost Sensing method, the measurement error is nearly 96.5%. When the signal segmentation reaches 16 segments, the experimental results gradually become closer to correct. Note that in *Range_1*, the experimental result of 128 segments reaches the best performance, while in *Range_2*, the experimental result of 256 segments reaches the best performance. These two numbers are exactly consistent with what we analyzed in Sec. IV-C2.

We further measure the average computation time on the correct signal segment. As shown in Fig. 33, the average computation time of RoLEX across different signal segments remains consistently below 0.45 s. This demonstrates that the Boost Sensing method does not pose a computational bottleneck for RoLEX. With its negligible impact on processing time, the proposed Boost Sensing method enables RoLEX to achieve accurate measurements of high-frequency motion targets while maintaining real-time performance.

TABLE II
PERFORMANCE OF DIFFERENT OVERLAP RATIO

	0%	25%	50%	80%
Error (%)	3.5%	3.1%	2.8%	2.2%
Time	$0.57\times$	$0.71\times$	1×	$2.29\times$

TABLE III
COMPARISON RESULTS OF DIFFERENT SYSTEMS

	RoLEX	Wi-Rotate	mRotate	PCIAS
Distance (m)	50 m	3 m	2.5 m	0.8 m
Error (%)	0.75%	0.77%	0.28%	3%

3) *Overlapping Sliding Window*: In this experiment, we track the rotor's speed over a continuous 5-minute period using RoLEX, and investigate how different overlap ratios affect the performance. Specifically, we evaluate four overlap ratios: 0%, 25%, 50%, and 80%, to explore the trade-off between the 90th percentile tracking error and the processing time. All time values are reported relative to the 50% overlap configuration, which serves as the baseline (1×).

As shown in Tab. II, increasing the overlap ratio improves the tracking accuracy but also incurs additional processing time. The 90th percentile error decreases from 3.5% (no overlap) to 2.2% (with 80% overlap), demonstrating the benefit of finer-grained temporal resolution in capturing dynamic speed variations. Notably, a 50% overlap already achieves sufficient performance (2.8% error) with moderate processing time, achieving a balance between accuracy and efficiency. In contrast, 80% overlap improves accuracy but introduces a $2.29\times$ increase in processing time, which may not be appropriate for real-time measurement. These results suggest that moderate overlap ratio offers a good trade-off for robust and efficient rotation speed tracking. Overall, the overlap ratio is an effective lever to control the trade-off between sensing granularity and processing time, and RoLEX can be flexibly configured for different deployment scenarios.

F. Comparison with Previous Systems

In this section, we compare RoLEX with three previous rotation speed measurement systems, *i.e.*, Wi-Rotate [12], mRotate [4], and PCIAS [1], focusing on their effective measurement distance and average measurement error when distance is 0.8 m. As shown in Tab. III, RoLEX demonstrates a significant advantage in measurement distance, reaching up to 50 m, compared to 3 m for Wi-Rotate, 2.5 m for mRotate, and only 0.8 m for PCIAS. This improvement is achieved by concentrating the energy of the reflected signal to enhance the SNR, enabling ultra-long-distance rotation speed measurement. In contrast, other systems directly process raw signals, limiting their effective sensing distance.

Regarding measurement accuracy, PCIAS performs the worst, with an error of 3%, due to its acoustic-based approach being highly susceptible to environmental noise. The RF-based systems, including RoLEX, Wi-Rotate, and mRotate, achieve much higher accuracy, all with errors below 0.8%. Specifically, RoLEX and Wi-Rotate have similar accuracy at around 0.75%, while mRotate achieves the best accuracy with an error of 0.28%. Although RoLEX's accuracy is slightly lower than mRotate, its measurement error remains well within

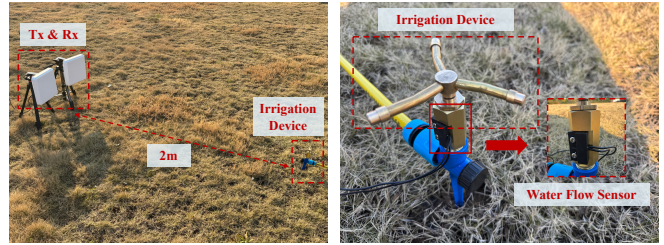


Fig. 34. Experimental Scenario

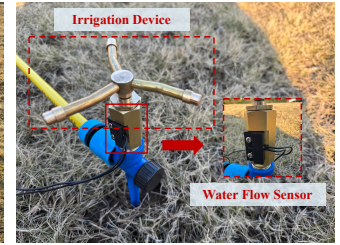


Fig. 35. Details on the Device Side

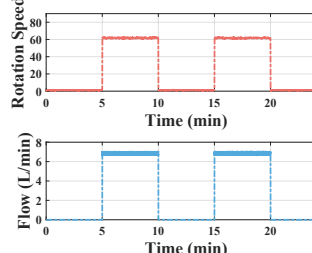


Fig. 36. Monitoring Results

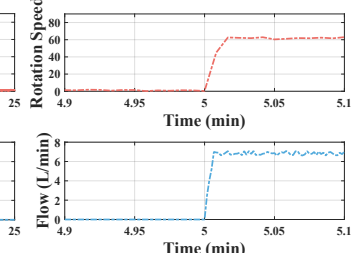


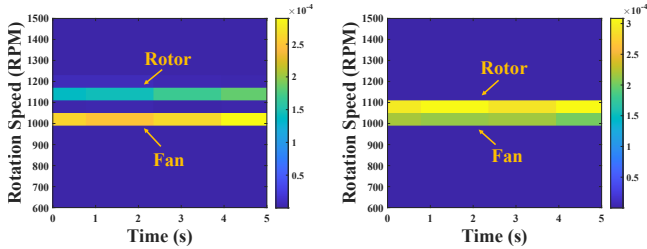
Fig. 37. Results Details at Startup

the acceptable range for daily use, and its unparalleled sensing range makes it highly effective for practical applications.

VI. CASE STUDY

In this section, we present a case study to showcase the practical deployment and effectiveness of RoLEX in monitoring a rotary irrigation device operating on lawns. The experimental setup is illustrated in Fig. 34. The transceiver is deployed 2 m away from the irrigation device at a measurement angle of approximately 60 degrees. The irrigation device, as shown in Fig. 35, is a three-pronged, water-driven sprinkler with a rotating diameter of 7 inches. To accurately capture changes in water flow, we install a water flow sensor under the sprinkler, whose sampling rate is 10 Hz. We pre-measure the rotation speed and water flow of the sprinkler during normal operation with the laser tachometer and the water flow sensor, which are 62.71 RPM and 7.1 L/min, respectively. Note that the water flow sensor is rated at 0.3 L/min to 10 L/min, meaning if there is no water flowing through, the sensor reads 0.

We deploy RoLEX to monitor the irrigation device continuously for 25 minutes, with the device being activated at 5-minute intervals, each operation lasting for 5 minutes. The experimental results are shown in Fig. 36 and Fig. 37. Overall, as shown in Fig. 36, RoLEX effectively monitors changes in the rotation speed of the sprinkler and correlates these changes with water flow variations almost synchronously. The average error of RoLEX in measuring rotation speed is about 1.67%. To further analyze system performance during startup, Fig. 37 details the transition to the sprinkler's stable working state. The water flow sensor indicates that the irrigation device stabilizes approximately 0.4 s after startup. In comparison, RoLEX calculates rotation speed at a frequency of 2 Hz, leading to a detection delay relative to the water flow sensor. However, as shown in Fig. 37, RoLEX needs 1 s to detect the stable working state of the device, which is only about 0.6 s later than the sensor. These results validate that RoLEX can monitor rotary irrigation devices in near real-time, effectively reducing the need for additional sensors while providing reliable performance.



(a) Results with Time Window of 1 s (b) Results with Time Window of 3 s
Fig. 38. Results of Multi-Target Measurement

VII. DISCUSSION

A. Dealing with Multi-Target Scenario

Contactless multi-target sensing is a well-known challenge because signal reflections from multiple targets get mixed at the receiver. Separating these signals typically demands either a wide frequency bandwidth in the time domain or a large antenna array in the spatial domain. However, LoRa is a well-known narrowband signal with a maximum bandwidth of 500 kHz and RoLEX uses only one pair of antennas to transmit and receive signals. Therefore, measuring multi-rotating targets simultaneously remains a challenge for RoLEX.

We further evaluate the multi-target measurement performance of RoLEX by simultaneously measuring the rotation speed of the fan and the rotor. The distance between them is 0.4 m and the measurement distance is 7 m. As illustrated in Fig. 38, when facing targets with different rotation speeds, RoLEX can obtain the rotation speed of each target from the frequency spectrum. Specifically, with the time window selected as 1 s, RoLEX could distinguish two targets with a speed difference of 100 RPM. When extending the time window to 3 s, RoLEX could differentiate two targets with a speed difference of 60 RPM.

However, when measuring multiple targets with similar rotation speeds, RoLEX may struggle to distinguish the rotation speeds of different targets in the spectrum. Recently, Zhang *et al.* [21] utilized beamforming to enable multi-target respiration sensing with LoRa. This inspires us to achieve rotation speed measurement of multi-targets, which is our future work.

In summary, while RoLEX faces challenges in measuring multiple targets with similar speeds or weak spatial separation, our experimental results demonstrate promising initial capabilities, and we see multi-target generalization as a compelling direction for future enhancement.

B. Dealing with Compatibility with Commercial Equipment

In this paper, RoLEX is implemented on USRP platforms with a high sampling rate (1 MHz) and Tx/Rx synchronization. While this setup facilitates system evaluation, it differs from low-cost LoRa nodes, which may experience issues such as frequency drift and phase jitter. Fortunately, recent studies [17], [18] have proposed compensation strategies for carrier frequency offset (CFO) and sampling frequency offset (SFO), which can ensure sensing performance even in the case of independent transmitters and receivers.

Furthermore, modern LoRa gateways [30] often integrate edge processors such as Raspberry Pi, enabling direct access

TABLE IV
COMPARISON OF COMPUTATIONAL OVERHEAD

	Raspberry Pi		i7-1260P	
	Time (s)	Memory (MB)	Time (s)	Memory (MB)
Xcorr	0.803 s	44.67 MB	0.134 s	23.18 MB
FFT	0.015 s	1.48 MB	0.001 s	0.03 MB
Threshold	0.013 s	—	0.006 s	—

to physical-layer I/Q samples and on-device signal processing. To validate the feasibility of real-world integration, we benchmarked the three core functional modules of RoLEX, *i.e.*, cross-correlation (Xcorr), FFT, and adaptive threshold, on both a Raspberry Pi 4B (4 GB RAM) and an Intel i7-1260P CPU with python. We measured their runtime and memory usage, as summarized in Tab. IV.

Results show that even on the Raspberry Pi, the most computationally demanding operation (Xcorr) only requires 0.803 s and less than 45 MB memory per measurement, while FFT and thresholding incur negligible cost. Though the Python implementation runs roughly six times faster on the CPU, the overall processing time on the Raspberry Pi remains sub-second, demonstrating that the system is lightweight enough for low-power embedded platforms. Moreover, compared with our MATLAB-based implementation (Sec. V-D), the Python implementation is more lightweight and better aligned with practical embedded deployment, since it can take advantage of optimized numerical libraries and low-level hardware acceleration. Together with our detailed analysis in Sec. V-D, these findings confirm that RoLEX remains lightweight, and its core pipeline can be efficiently deployed on commercial LoRa gateways and other low-power IoT devices.

In our future work, we plan to build a fully integrated prototype on commodity LoRa gateways and address practical issues such as frequency drift and phase jitter for robust deployment. We will also explore lightweight calibration and adaptive processing strategies to improve robustness under diverse environments, thereby enhancing the practicality and scalability of RoLEX in real-world IoT scenarios.

C. Dealing with Large Scale Interference

As introduced in Sec. V-B5, RoLEX is robust to slight environmental interference. However, if someone makes large-scale interfering movements near RoLEX, the measurement accuracy will drop rapidly. Note that once the large-scale interference disappears, the accuracy of RoLEX can be restored instantly. Since RoLEX mainly collects signals reflected by the target for measurement, the reflected energy of large-scale interference is much stronger than the energy of the target, which will lead to a serious decrease in measurement accuracy. However, when measuring large motors in industrial scenarios, there is usually no large-scale interference around for safety reasons. Therefore, the measurement accuracy of RoLEX is guaranteed at this time. In our future work, inspired by methods in [13] and [16], we can take similar methods to eliminate interference for accurate measurement.

D. Dealing with the Boundary Frequency

In Range_2, RoLEX uses LoRa_30 to measure high-frequency rotation speeds, avoiding the strong boundary fre-

quency interference that occurs with *LoRa_60* in this range. Our current approach partitions the speed range and selects LoRa signals whose boundary frequencies lie outside the target measurement range, effectively mitigating aliasing effects and simplifying peak identification in the frequency spectrum. However, this design requires signal switching when the measured speed crosses range boundaries, which may introduce overhead and complexity. To address this limitation, our future work will combine advanced time-frequency analysis [1], [12] with machine learning techniques [31] to separate overlapping frequency components and accurately measure rotation speed using only one kind of LoRa signal. Such improvements will enhance the measurement efficiency and system adaptability, enabling RoLEX to operate seamlessly across the full speed ranges without signal switching, thus supporting more flexible and scalable deployments.

E. Dealing with Different Environmental Factors

Besides physical obstructions and interference, various environmental factors may also affect the measurement performance of RoLEX. For example, changes in temperature or humidity can slightly alter the dielectric properties of the surrounding medium, potentially impacting the propagation characteristics of LoRa signals. Similarly, mechanical vibrations in the vicinity of the rotating object, or reflective surfaces near the device, may introduce additional multipath effects or phase jitter. Although our current experiments were conducted under relatively controlled indoor conditions, we note that RoLEX demonstrated consistent performance in a range of scenes, including rooms with metal equipment (Sec. V-B1), walls (Sec. V-B6), and multiple rotating objects (Sec. VII-A). To improve generalizability in more complex environments (*e.g.*, outdoors or high-humidity scenarios), RoLEX can benefit from adaptive signal filtering [32] and multi-instance temporal smoothing [1], which we leave as future work.

VIII. RELATED WORK

Wireless-based sensing techniques. Various wireless technologies are extensively utilized for sensing applications, including millimeter-wave radar [33]–[36], Doppler radar [37], [38], UWB radar [39], [40], FMCW radar [41], commodity WiFi [42]–[46], RFID [47]–[49], acoustic [32], [50]–[52], and sensors [53], [54]. For instance, Zhang *et al.* [44] utilized commodity Wi-Fi devices to detect human respiration from distances of 2 - 4 meters. Wan *et al.* [50] exploited the sensitivity of acoustic signals to temperature changes and proposed a temperature field sensing system for accurate temperature monitoring. Although these wireless sensing techniques have broad prospects, their sensing distances are limited. In this paper, we introduce RoLEX, a system proposed for contactless rotation speed sensing, along with solutions aimed at significantly extending the sensing distance.

LoRa-based communication and sensing techniques. In recent years, there has been notable advancement in LoRa communication [19], [55], [56]. Previous studies predominantly focus on utilizing LoRa's long-distance communication capability for tasks such as sensor data transmission [57], [58]

and device localization [59]–[61]. However, there is a growing interest in exploiting the LoRa signal itself as a potent sensing tool [13], [14], [62], [63]. Zhang *et al.* [18] introduced the signal ratio scheme, achieving a sensing distance of 25 m for respiration sensing, and utilized beamforming to enable multi-target respiration sensing [21]. Subsequently, Xie *et al.* [17] extended the range for respiration sensing to approximately 70 m. These studies underscore the potential of LoRa signals for sensing tasks, albeit primarily in low-frequency motion scenarios. Thanks to proposed signal processing techniques, RoLEX can now effectively sense high-frequency motion, expanding its applicability to diverse scenarios.

Rotation speed measurement techniques. Existing systems for measuring rotation speed can be broadly categorized into contact-based and contactless systems. Contact-based systems [8] are physically affixed to the shaft of the target object, limiting their operational distances and potentially posing safety risks to operators. In contrast, contactless systems [1], [4], [12], [64] offer greater flexibility as they do not require direct attachment to the target. Li *et al.* [1] utilized acoustic signals to extract various signal features across different rotation speed ranges, enabling the measurement of instantaneous angular velocity, while Lin *et al.* [12] developed a rotation speed measurement system utilizing commodity WiFi with a measurement distance up to 3 m. We posit that RoLEX offers a valuable complement to existing systems by providing longer sensing distance (50 m) and a wider range of rotation speeds (100 RPM-5100 RPM) for measurement compared to the previous systems.

IX. CONCLUSION

In this paper, we propose RoLEX, a LoRa-based rotation speed measurement system for long-distance and contactless monitoring of rotating machinery in ubiquitous scenarios. RoLEX employs a novel Signal Selection method to eliminate chirp interference and adapt to varying rotation speeds, along with a Boost Sensing method to enhance sampling rates and an advanced feature processing algorithm for precise rotation speed estimation and tracking. Extensive experiment results demonstrate that RoLEX is robust to interference and obstructions and achieves a measurement distance of 50 m, with an average measurement error less than 0.69% across different rotation speeds and a relative error less than 2.8% in 90% of cases for rotation speed tracking.

REFERENCES

- [1] Z. Li *et al.*, “PCIAS: Precise and Contactless Measurement of Instantaneous Angular Speed Using a Smartphone,” *ACM IMWUT*, vol. 2, no. 4, pp. 1–24, 2018.
- [2] The Portable Laundry, “Rpm in washing machine,” <https://theportablelaundry.com/washing-machine-rpm/>.
- [3] B. Li *et al.*, “Measurement of Instantaneous Angular Displacement Fluctuation and its applications on gearbox fault detection,” *ISA Transactions*, vol. 74, pp. 245–260, 2018.
- [4] R. Ding *et al.*, “Rotation speed sensing with mmwave radar,” in *IEEE INFOCOM*, 2023, pp. 1–10.
- [5] L. Li *et al.*, “Digital Approach to Rotational Speed Measurement Using an Electrostatic Sensor,” *Sensors*, vol. 19, no. 11, 2019.
- [6] Uwoodcraft, “Turning lathe speeds,” 2019, <https://uwoodcraft.com/woodturning-lathe-speeds-a-complete-guide/>.

- [7] Haynes, “Vehicle inspections,” <https://haynes.com/en-us/tips-tutorials/what-know-about-vehicle-inspections-all-50-states>.
- [8] REED Instruments, “Photo-contact tachometer instruction manual,” <https://www.reedinstruments.com/pdfs/cache/www.reedinstruments.com/r7100/manual/r7100-manual.pdf>.
- [9] J. Kathirvelan *et al.*, “Hall Effect Sensor Based Portable Tachometer for RPM Measurement,” *International Journal on Computer Science and Engineering*, vol. 2, pp. 100–105, 2014.
- [10] Y. Wang *et al.*, “Rotational speed measurement through digital imaging and image processing,” in *IEEE I2MTC*, 2017, pp. 1–6.
- [11] T. Wang *et al.*, “Rotational speed measurement through image similarity evaluation and spectral analysis,” *IEEE Access*, vol. 6, pp. 46718–46730, 2018.
- [12] C. Lin *et al.*, “Wi-Rotate: An Instantaneous Angular Speed Measurement System Using WiFi Signals,” *IEEE Transactions on Mobile Computing*, vol. 23, no. 1, pp. 985–1000, 2024.
- [13] B. Xie *et al.*, “Boosting the Long Range Sensing Potential of LoRa,” in *ACM MobiSys*, 2023, pp. 177–190.
- [14] Z. Chang *et al.*, “Sensor-free Soil Moisture Sensing Using LoRa Signals,” *ACM IMWUT*, vol. 6, no. 2, pp. 45:1–45:27, 2022.
- [15] G. Ciattaglia *et al.*, “UAV Propeller Rotational Speed Measurement through FMCW Radars,” *Remote Sensing*, vol. 15, no. 1, p. 270, 2023.
- [16] B. Xie and J. Xiong, “Combating Interference for Long Range LoRa Sensing,” in *ACM SenSys*, 2020, p. 69–81.
- [17] B. Xie *et al.*, “Pushing the Limits of Long Range Wireless Sensing with LoRa,” *ACM IMWUT*, vol. 5, no. 3, 2021.
- [18] F. Zhang *et al.*, “Exploring LoRa for Long-Range Through-Wall Sensing,” *ACM IMWUT*, vol. 4, no. 2, pp. 1–27, 2020.
- [19] C. Li *et al.*, “NELoRa: Towards Ultra-low SNR LoRa Communication with Neural-enhanced Demodulation,” in *ACM SenSys*, 2021, pp. 56–68.
- [20] Y. Peng *et al.*, “PLoRa: a passive long-range data network from ambient LoRa transmissions,” in *ACM SIGCOMM*, 2018, pp. 147–160.
- [21] F. Zhang *et al.*, “Unlocking the Beamforming Potential of LoRa for Long-range Multi-target Respiration Sensing,” *ACM IMWUT*, vol. 5, no. 2, pp. 85:1–85:25, 2021.
- [22] C. Ozdemir, *Inverse synthetic aperture radar imaging with MATLAB algorithms*. John Wiley & Sons, 2012.
- [23] Semtech, “LoRa Technology,” 2024, <https://www.semtech.com/lora>.
- [24] M. Shang and J. Liu, “Sampling Methods in Multi-objective optimization Algorithm of Electric Motors Based on Approximate Metamodel,” in *IEEE ICEMS*, 2023, pp. 602–606.
- [25] J. Liu and Q. Wang, “A High-performance Digital Automatic Voltage Regulator for Brushless Wound Excited Synchronous Generator On-Vehicle and Its implementation,” in *IEEE ICEMS*, 2022, pp. 1–4.
- [26] Gnu Radio, “Gnu radio library,” <https://www.gnuradio.org/>.
- [27] U-T. Technology, “Laser tachometer operating manual,” <https://meters.uni-trend.com/product/ut370-series/#Docs/>.
- [28] W. P. N. dos Reis *et al.*, “Direct current geared motor data: Voltage, current, and speed measured under different experimental conditions,” *Data in Brief*, vol. 40, p. 107802, 2022.
- [29] S. Pu *et al.*, “Study on dynamic characteristics of rotor-bearing system under pitching condition,” *Journal of Physics: Conference Series*, vol. 2113, no. 1, p. 012021, 2021.
- [30] Semtech, “LoRa Gateway SX1257,” 2024, <https://www.semtech.com/products/wireless-rf/lora-core/sx1257>.
- [31] H. Dahrouj *et al.*, “An Overview of Machine Learning-Based Techniques for Solving Optimization Problems in Communications and Signal Processing,” *IEEE Access*, vol. 9, pp. 74908–74938, 2021.
- [32] L. Wang *et al.*, “DF-Sense: Multi-user Acoustic Sensing for Heartbeat Monitoring with Dualforming,” in *ACM MobiSys*, 2023, pp. 1–13.
- [33] Z. Yang *et al.*, “Monitoring vital signs using millimeter wave,” in *ACM MobiHoc*, 2016, pp. 211–220.
- [34] C. Wang *et al.*, “mmEve: eavesdropping on smartphone’s earpiece via COTS mmwave device,” in *ACM MobiCom*, 2022, pp. 338–351.
- [35] H. Xue *et al.*, “Towards Generalized mmWave-based Human Pose Estimation through Signal Augmentation,” in *ACM MobiCom*, 2023, pp. 88:1–88:15.
- [36] W. Zhang *et al.*, “mP-Gait: Fine-grained Parkinson’s Disease Gait Impairment Assessment with Robust Feature Analysis,” *ACM IMWUT*, vol. 8, no. 3, pp. 1–31, 2024.
- [37] M. Nowogrodzki *et al.*, “Non-invasive microwave instruments for the measurement of respiration and heart rates,” *NAECON 1984*, pp. 958–960, 1984.
- [38] K. Jiang *et al.*, “A single dwell velocity estimation method for pulse Doppler radar using multicarrier signals,” *Signal Processing*, vol. 217, p. 109324, 2024.
- [39] Z. L. aand others, “WISE: Low-Cost Wide Band Spectrum Sensing Using UWB,” in *ACM SenSys*, 2022, pp. 651–666.
- [40] T. Zheng *et al.*, “MoRe-Fi: Motion-robust and Fine-grained Respiration Monitoring via Deep-Learning UWB Radar,” in *ACM SenSys*, 2021, pp. 111–124.
- [41] F. Adib *et al.*, “Smart Homes that Monitor Breathing and Heart Rate,” in *ACM CHI*, 2015, pp. 837–846.
- [42] B. Sheng *et al.*, “MetaFormer: Domain-Adaptive WiFi Sensing with Only One Labelled Target Sample,” *ACM IMWUT*, vol. 8, no. 1, pp. 39:1–39:27, 2024.
- [43] F. Adib and D. Katabi, “See through walls with WiFi!” in *ACM SIGCOMM*, 2013, pp. 75–86.
- [44] F. Zhang *et al.*, “From Fresnel Diffraction Model to Fine-grained Human Respiration Sensing with Commodity Wi-Fi Devices,” *ACM IMWUT*, vol. 2, no. 1, pp. 53:1–53:23, 2018.
- [45] L. Wang *et al.*, “WiTrace: Centimeter-Level Passive Gesture Tracking Using OFDM Signals,” *IEEE Transactions on Mobile Computing*, vol. 20, no. 4, pp. 1730–1745, 2021.
- [46] Y. Huang, “Challenges and Opportunities of Sub-6 GHz Integrated Sensing and Communications for 5G-Advanced and Beyond,” *Chinese Journal of Electronics*, vol. 33, no. 2, pp. 323–325, 2024.
- [47] J. Liu *et al.*, “Pose Sensing With a Single RFID Tag,” *IEEE/ACM Transactions on Networking*, vol. 28, no. 5, pp. 2023–2036, 2020.
- [48] J. Nolan *et al.*, “KeyStub: A Passive RFID-based Keypad Interface Using Resonant Stubs,” *ACM IMWUT*, vol. 7, no. 4, pp. 173:1–173:23, 2023.
- [49] Y. Lin *et al.*, “DropMonitor: Millimeter-level Sensing for RFID-based Infusion Drip Rate Monitoring,” *ACM IMWUT*, vol. 5, no. 2, pp. 72:1–72:22, 2021.
- [50] H. Wan *et al.*, “VECTOR: Velocity Based Temperature-field Monitoring with Distributedn Acoustic Devices,” *ACM IMWUT*, vol. 6, no. 3, pp. 144:1–144:28, 2022.
- [51] X. Wang *et al.*, “UltraCLR: Contrastive Representation Learning Framework for Ultrasound-based Sensing,” *ACM Transactions on Sensor Networks*, 2023.
- [52] Z. Li *et al.*, “PD-Gait: Contactless and Privacy-Preserving Gait Measurement of Parkinson’s Disease Patients using Acoustic Signals,” *SPE*, vol. 54, no. 9, pp. 1733–1753, 2024.
- [53] Y. Sun *et al.*, “Vibration-based Fault Diagnosis for Railway Point Machines using VMD and Multiscale Fluctuation-based Dispersion Entropy,” *Chinese Journal of Electronics*, vol. 33, no. 3, pp. 803–813, 2024.
- [54] C. Tang *et al.*, “Mobility Prediction based Tracking of Moving Objects in Wireless Sensor Networks,” *Chinese Journal of Electronics*, vol. 32, no. 4, pp. 793–805, 2023.
- [55] J. C. Liendo *et al.*, “Known and Unknown Facts of LoRa: Experiences from a Large-scale Measurement Study,” *ACM Transactions on Sensor Networks*, vol. 15, no. 2, pp. 16:1–16:35, 2019.
- [56] F. Yu *et al.*, “LoRadar: An Efficient LoRa Channel Occupancy Acquirer based on Cross-channel Scanning,” in *IEEE INFOCOM*, 2022, pp. 540–549.
- [57] T. Hossain *et al.*, “Activity Recognition by Using LoRaWAN Sensor,” in *ACM UbiComp*, 2018, pp. 58–61.
- [58] T. Hossain, Y. Doi *et al.*, “Study of LoRaWAN Technology for Activity Recognition,” in *ACM UbiComp*, 2018, pp. 1449–1453.
- [59] K. Hu *et al.*, “LTrack: A LoRa-Based Indoor Tracking System for Mobile Robots,” *IEEE Transactions on Vehicular Technology*, vol. 71, no. 4, pp. 4264–4276, 2022.
- [60] Y. Lin *et al.*, “SateLoc: A Virtual Fingerprinting Approach to Outdoor LoRa Localization Using Satellite Images,” *ACM Transactions on Sensor Networks*, vol. 17, no. 4, pp. 43:1–43:28, 2021.
- [61] J. Liu *et al.*, “Seiros: leveraging multiple channels for LoRaWAN indoor and outdoor localization,” in *ACM MobiCom*, 2021, pp. 656–669.
- [62] Y. Yin *et al.*, “MineSOS: Long-Range LoRa-Based Distress Gesture Sensing for Coal Mine Rescue,” in *Springer WASA*, vol. 13472, 2022, pp. 105–116.
- [63] H. Jiang *et al.*, “Sense Me on the Ride: Accurate Mobile Sensing over a LoRa Backscatter Channel,” in *ACM SenSys*, 2021, pp. 125–137.
- [64] G. Zhao *et al.*, “EV-Tach: A Handheld Rotational Speed Estimation System With Event Camera,” *IEEE Transactions on Mobile Computing*, vol. 23, no. 6, pp. 7483–7498, 2024.



Keran Li (Student Member, IEEE) received the B.E. degree from the Faculty of Electronic Information and Electrical Engineering, Dalian University of Technology in 2022. He is currently working towards the Ph.D. degree from the School of Computer Science and Technology, Nanjing University, Nanjing, China. His research interests focus on wireless sensing and mobile computing.



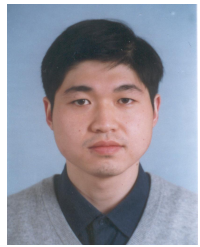
Shuai Tong received the B.E. degree from Nankai University, and the Ph.D. degree from Tsinghua University in 2024. He is currently a Post-Doctoral Researcher at Tsinghua University. His research interests include low-power wide-area networks and Internet of Things.



Haipeng Dai (Senior Member, IEEE) received the B.S. degree in the Department of Electronic Engineering from Shanghai Jiao Tong University in 2010, and the Ph.D. degree in the Department of Computer Science and Technology in Nanjing University in 2014. He is IEEE and ACM member. He is currently an associate professor of the School of Computer Science and Technology, Nanjing University. His research interests mainly include data mining, Internet of Things, and mobile computing.



Meng Li (Member, IEEE) received his B.S. degree in Computer Science from Nanjing University, Jiangsu, China, in 2016 and the Ph.D. degree in the Department of Computer Science and Technology in Nanjing University, Nanjing, China, in 2023. He is currently an assistant researcher at Nanjing University. His research interests are in the area of sketch-enabled high performance systems and network as well as IOT.



Wei Wang (Member, IEEE) received his M.S. and Ph.D. degree from the ESE department of Nanjing University and the ECE department of National University of Singapore, in 2000 and 2008 respectively. He is currently a Professor in the School of Computer Science and Technology, Nanjing University. His research interests are in the area of wireless networks, including Device-free Sensing, Cellular Network Measurements, and Software Defined Radio systems.



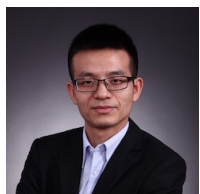
Lei Wang (Member, IEEE) received his Ph.D. degree from Department of Computer Science and Technology of Nanjing University, China, in April 2020. He was a postdoctoral fellow at School of Computer Science, Peking University, China, from September 2020 to November 2022. He is currently an Associate Professor at Soochow University, China. His research interests are in the areas of pervasive computing, wireless sensing.



Junlong Chen received the B.S. degree in the School of Computer Science and Technology from Harbin Institute of Technology in 2023. He is currently working toward the M.S. degree in the School of Computer Science and Technology, Nanjing University. His research interests include deep learning and machine learning, wireless sensing and mobile computing.



Haoran Wang is currently pursuing the B.S. degree in Computer Science and Technology from Nanjing University. His research interests include wireless sensing and mobile computing.



Jiliang Wang (Senior Member, IEEE) received the B.E. degree in computer science and technology from the University of Science and Technology of China, Hefei, China, and the Ph.D. degree in computer science and engineering from The Hong Kong University of Science and Technology, Hong Kong. He is currently an associate professor with the School of Software and BNRIst, Tsinghua University, Beijing, China. His research interests include wireless networks, the Internet of Things, and mobile computing.



Guanghai Chen (Fellow, IEEE) received the B.S. degree from Nanjing University, Nanjing, China, the M.E. degree from Southeast University, Nanjing, China, and the Ph.D. degree from the University of Hong Kong, Hong Kong. He visited the Kyushu Institute of Technology, Japan, in 1998, as a research fellow, and the University of Queensland, Australia, in 2000, as a visiting professor. From 2001 to 2003, he was a visiting professor with Wayne State University. He is currently a distinguished professor and a deputy chair with the Department of Computer Science, Shanghai Jiao Tong University. His research interests include wireless sensor networks, peer-to-peer computing, and performance evaluation.